Long-term morphodynamic evolution of a tidal embayment using a two-dimensional, process-based model

M. van der Wegen[1] and J. A. Roelvink[1,2]

Received 19 October 2006; revised 18 October 2007; accepted 25 October 2007; published 14 March 2008.

[1] The research objective is to investigate long-term evolution of estuarine morphodynamics with special emphasis on the impact of pattern formation. Use is made of a two-dimensional (2-D), numerical, process-based model. The standard model configuration is a rectangular 80 km long and 2.5 km wide basin. Equilibrium conditions of the longitudinal profile are analyzed using the model in 1-D mode after 8000 years. Two-dimensional model results show two distinct timescales. The first timescale is related to pattern formation taking place within the first decades and followed by minor adaptation according to the second timescale of continuous deepening of the longitudinal profile during 1600 years. The resulting longitudinal profiles of the 1-D and 2-D runs are similar apart from small deviations near the mouth. The 2-D results correspond well to empirically derived relationships between the tidal prism and the channel cross section and between the tidal prism and the channel volume. Also, comparison between the current model results and data from the Western Scheldt estuary (in terms of bar length, hypsometry, percentage of intertidal area and values for the ratio of shoal volume and channel volume against the ratio of tidal amplitude and water depth) shows satisfying agreement. On the basis of the model results a relationship for a characteristic morphological wavelength was derived on the basis of the tidal excursion and the basin width and an exponentially varying function was suggested for describing a dimensionless hypsometric curve for the basin. Furthermore, special attention is given to an analysis of the numerical morphodynamic update scheme applied.

Citation: van der Wegen, M., and J. A. Roelvink (2008), Long-term morphodynamic evolution of a tidal embayment using a two-dimensional, process-based model, *J. Geophys. Res.*, *113*, C03016, doi:10.1029/2006JC003983.

1. Introduction

[2] Estuaries are valuable areas of both local and international importance. Breeding fish and migrating birds are only examples of the estuarine ecosystem richness. From an economic point of view, local fishery, aquaculture and tourism are important sectors that profit from the estuarine environment. Additionally, numerous ports situated along estuaries form the logistical link between ocean transport and the hinterland.

[3] The morphology of estuaries is closely linked to these estuarine values. Tidal flats and salt marshes are essential in providing food for migrating birds and stimulate local flora and fauna. At the same time, the channel system provides natural access to ports, although in many cases regular dredging is required to allow a sustainable access for sea vessels with increasing draughts. It is thus of major importance to develop insight into the morphodynamic processes in an estuary in order to estimate impacts of, for example, human interference (i.e., land reclamation and dredging) and sea level rise.

[4] Phenomenological descriptions of estuarine morphology are given by *Van Veen* [1936, 1950] and *Ahnert* [1960]. Additionally, *O'Brien* [1969], *Jarret* [1976] and *Eysink* [1990] present empirical relationships between the minimum cross-sectional area of a tidal channel and the tidal prism through this cross section based on estuarine data along the U.S. coast and the Waddenzee, the Netherlands. These relationships assume morphodynamic equilibrium, but do not explain the origin of the equilibrium and its sensitivity to changing conditions. Only few researches were carried out in the laboratory investigating equilibrium conditions. *Tambroni et al.* [2005] investigated equilibrium conditions of the width-averaged longitudinal bed profile for both a rectangular basin and a basin with an exponentially decaying width. They found good agreement with earlier results from a width-averaged one-dimensional (1-D) mathematical model by *Lanzoni and Seminara* [2002].

[5] With respect to pattern formation, *Schuttelaars and De Swart* [1999], *Seminara and Tubino* [2001], *Schramkowski et al.* [2002] and *Van Leeuwen and De Swart* [2004] describe initial channel/shoal formation in a highly schematized tidal environment. They found that dominant morphological wavelengths are determined by an approximate balance between the destabilizing divergence of the sediment transport field and the stabilizing divergence of sediment fluxes induced by the presence of a bed slope.

[1] UNESCO-IHE Institute for Water Education, Delft, Netherlands.
[2] Also at WL|Delft Hydraulics, Delft, Netherlands.

0148-0227/08/2006JC003983

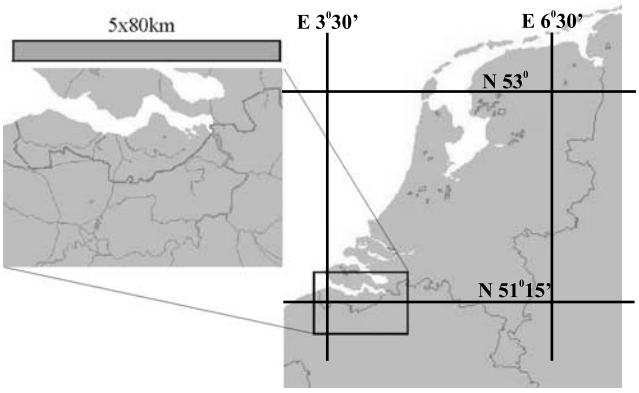

Figure 1. Western Scheldt estuary, the Netherlands and Belgium (source: Rijkswaterstaat Data-ICT-Dienst, Delft, Netherlands).

Typical feature of the initially developing bars is that they can be related to the (short) basin length, the embayment width and the relative importance of diffusive and advective transports [*Van Leeuwen and De Swart*, 2004], or the tidal excursion length implicitly taking into account the impact of friction and depth [*Schramkowski et al.*, 2002]. Also, the sensitivity to diffusive or advective transports was investigated by *Van Leeuwen and De Swart* [2004]. As the bars grow in height, the effect of the bed slope on the bed load transport will be more pronounced. Additionally, there will be a more impact of nonlinear interactions between the bed and the hydrodynamics. *Coevelt et al.* [2003] concluded, on the basis of 3-D hydrodynamic calculations, that secondary flow (so called "spiral flow") in bends is of minor importance. *Schramkowski et al.* [2004] came to similar conclusions stating that a 2-D flow description suffices for long-term bar formation so that detailed 3-D model descriptions would not be necessary. The latter research pointed additionally to different types of equilibrium conditions for finite amplitude morphological waves (stable, periodically stable and unstable). Although they investigated the possible stability of specific morphological features, they did not conclude on a possible final equilibrium state of the channel/shoal system. Long-term, 2-D, simulations by *Hibma et al.* [2003b, 2003c] show stable patterns that have a characteristic length scale with an order of magnitude of the tidal excursion, although they are found to be 10% longer than the bars that emerge initially. This is attributed to the higher velocities in the channels between the bars.

[6] Equilibrium of the longitudinal width-averaged bed level was investigated extensively using 1-D models, which describe the propagation of a tidal wave into the estuary and relate this to morphodynamic conditions like equilibrium or ebb or flood dominance. For example, *Boon and Byrne* [1981] and *Friedrichs and Aubrey* [1988], pointed to the importance of the storage of tidal water on shoals and the interaction of the M_2 and M_4 tidal constituents (the latter also by *Schuttelaars and De Swart* [1996, 2000] and by *Hibma et al.* [2003a]). *Friedrichs and Aubrey* [1996] investigated separated effects of tides and waves. *Schuttelaars and De Swart* [1996, 2000] pointed to the relative importance of advective and diffusive transports and of the basin length itself. Finally, *Lanzoni and Seminara* [2002] stressed the impact of the (funnel) shape of the estuary.

[7] On the basis of the foregoing, two main considerations are put forward. First, pattern formation and longitudinal equilibrium profiles have been investigated separately. By definition, 1-D models do not take into account a laterally nonuniform velocity distribution due to shoals and channels present in a cross section. Considering that sediment transport depends faster than linear on the velocity, it is expected that channel/shoal patterns will at some stage impact on bed evolution and the (assumed) equilibrium conditions. Only *Hibma et al.* [2003b] investigated both aspects in parallel using a 2-D process-based model, although the focus of that study was on the pattern formation. Secondly, the empirical relationship derived by *O'Brien* [1969], *Jarret* [1976] and *Eysink* [1990] as well as the 1-D models suggest that equilibrium is present, despite the fact that especially the sediment transport is a highly nonlinear processes.

[8] The main aim of the current research is to investigate the characteristics of morphodynamic evolution in a tidal embayment, based on the application of a 2-D numerical, process-based model. This allows for a prediction of the evolution based on the inclusion of detailed hydrodynamic and morphodynamic processes. For example, it combines processes like pattern formation and profile evolution including their mutual dependency and different timescales and spatial scales. Simplifications are made in the model to make comparison with earlier research possible and to be able to analyze the results in a relatively straightforward way. These simplifications are mainly related to the sediment transport formulation and the model configuration. In order to validate the model results, emphasis is put on comparison with data from the Western Scheldt estuary, see Figure 1, so that the model configurations are based on dimensions similar to this estuary.

[9] The main aim of the study is systematically addressed by a number of more specific research questions. First question is related to the evolution characteristics of the longitudinal profile in a 1-D schematization, so that evolution can be studied for a relatively simple configuration. Second question considers the evolution and behavior of different 2-D schematizations, including an analysis of the different timescales and spatial scales in the evolution. Thirdly, it is questioned to what extent the 2-D model results compare with empirical relationships and data from the Western Scheldt estuary. Final research question is in how far 1-D and 2-D results coincide and what the reason might be for possible differences. In the analysis special emphasis is put on a discussion of the performance of the applied morphological update scheme.

[10] The following sections will first describe the formulation of the hydrodynamic and morphodynamic model, which is basically the same for the 1-D and 2-D schematizations. Secondly, the model results are presented for the 1-D schematization, the 2-D schematization, their comparison with each other and with empirical relationships and data from the Western Scheldt estuary. Finally, the modeling approach and results will be discussed in more detail.

2. Model

[11] The current research applies a process-based model described by *Lesser et al.* [2004] in which a detailed

description of the applied hydrodynamic equations, numerical aspects, as well as some elaborated test cases can be found. However, the focus in the work by *Lesser et al.* [2004] is on a description of the 3-D mode, although it also includes a comparison of the model run in 2-D (depth averaged) and 3-D mode for some case studies. Since the current model is 2-D depth-averaged, in the following sections the main model characteristics, will be described. This concerns, first, the governing hydrodynamic equations and, secondly, the formulations describing sediment transport and bed level update.

2.1. Hydrodynamic Model

[12] The hydrodynamic model is unsteady and two-dimensional and is based on the set of shallow water equations, in which vertical velocities are neglected. Neglecting the influence of the Coriolis force, density differences, wind and waves, the two-dimensional equation of continuity and the momentum equations read as follows:

$$\frac{\partial \zeta}{\partial t} + \frac{\partial h\overline{u}}{\partial x} + \frac{\partial h\overline{v}}{\partial y} = 0 \tag{1}$$

$$\frac{\partial \overline{u}}{\partial t} + \overline{u}\frac{\partial \overline{u}}{\partial x} + \overline{v}\frac{\partial \overline{u}}{\partial y} + g\frac{\partial \zeta}{\partial x} + c_f \frac{\overline{u}\sqrt{\overline{u}^2 + \overline{v}^2}}{h} - \nu_e\left(\frac{\partial^2 \overline{u}}{\partial x^2} + \frac{\partial^2 \overline{u}}{\partial y^2}\right) = 0 \tag{2}$$

$$\frac{\partial \overline{v}}{\partial t} + \overline{v}\frac{\partial \overline{v}}{\partial y} + \overline{u}\frac{\partial \overline{v}}{\partial x} + g\frac{\partial \zeta}{\partial y} + c_f \frac{\overline{v}\sqrt{\overline{u}^2 + \overline{v}^2}}{h} - \nu_e\left(\frac{\partial^2 \overline{v}}{\partial x^2} + \frac{\partial^2 \overline{v}}{\partial y^2}\right) = 0 \tag{3}$$

with

$$c_f = g\frac{n^2}{\sqrt[3]{h}} \tag{4}$$

in which

- ζ water level with respect to datum, m;
- h water depth, m;
- $\overline{u}$ depth averaged velocity in x direction, m/s;
- $\overline{v}$ depth averaged velocity in y direction, m/s;
- g gravitational acceleration, m^2/s;
- c_f friction coefficient;
- n Manning's coefficient, $sm^{-1/3}$;
- ν_e eddy viscosity, m^2/s.

2.2. Morphodynamic Model

2.2.1. Sediment Transport Formulation

[13] The velocity field obtained by solving the equation of continuity and the momentum equations is used to calculate the sediment transport field. Various sediment transport formulations are available for this in literature. *Van Leeuwen and De Swart* [2004] and *Schuttelaars and De Swart* [1996, 2000] indicated the different character of a 1-D equilibrium profile for different values of diffusive and/or advective transports. Further, on the basis of a literature review, *Lanzoni and Seminara* [2002] extensively analyze and describe dominant sediment transport processes in tidal environments. These are (a.o.) the presence of multiple sediment fractions including sand and mud, tidal asymmetries in currents and water levels resulting in continuously changing suspended sediment concentration profiles during the tidal cycle and erosion and settling lags particularly relevant at shoals around slack tide. Despite the recognition of these processes, for their model *Lanzoni and Seminara* [2002] finally choose for formulations of the bed and suspended load transports based on local and instantaneous flow conditions, because their analysis showed that these formulations would be justified at least in terms of leading order effects.

[14] The current research follows this reasoning and the authors, additionally, choose for a relatively simple transport formulation without making distinction between suspended load and bed load. Thus results could be analyzed in a more straightforward way whereas future research should focus on more complex transport formulations. Further support to the application of a total transport formulation is found by carrying out an analysis of transport and sedimentation scales. Assuming that advection dominates diffusive transports and a water depth (h) of 8 m, a characteristic flow velocity (u) of 1 m/s and a fall velocity (w) of 0.02 m/s, the length (dx) for a sediment particle at the surface to settle at the bed and being advected by the flow at the same time is dx = hu/w = 400 m. This value is an upper value considering that suspensive sediment is mainly concentrated in the lower part of the water column, that the water depth is lower than 8 m in large parts of the current basin and that velocities are typically lower than 1 m/s during the tidal cycle. In the current model a grid cell size of 62.5 m × 125 m is applied, because the grid should be able to resolve the characteristic length scales of the patterns which are expected to develop. It is assumed that this model grid size still covers the settling and erosion lags. This is supported by the observation that preliminary calculations including distinct formulations for the bed load and suspensive load [e.g., *Van Rijn*, 1993] indicate no large differences from results based on the current Engelund-Hansen formulation.

[15] Use is made of the instantaneous total sediment transport formula developed by *Engelund and Hansen* [1967] that relates velocity directly and locally to a sediment transport:

$$S = S_b + S_s = \frac{0.05U^5}{\sqrt{g}C^3\Delta^2 D_{50}} \tag{5}$$

where

- S magnitude of the sediment transport, m^3/ms;
- S_b, S_s magnitude of the bed load and suspended load transport, m^3/ms;
- U magnitude of flow velocity, m/s;
- Δ relative density $(\rho_s - \rho_w)/\rho_w$;
- C friction parameter defined by $\frac{\sqrt[6]{h}}{n}$, $m^{1/2}/s$;
- n Manning's coefficient, $sm^{-1/3}$;
- D_{50} median grain size, m.

2.2.2. Bed Slope Effect

[16] Usually, distinction is made between bed load and suspended load, where the effect of the bed slope on the bed load transport is at least an order of magnitude larger than

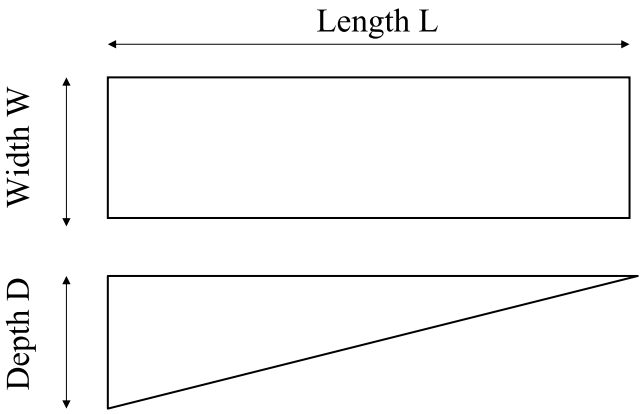

Figure 2. (top) Map and (bottom) longitudinal cross section of standard model configuration where W is basin width and L is basin length.

the bed slope effect on the suspended load transport. However, the current model does not distinguish between bed load and suspended load since a total sediment transport formula is used. Also, the current model uses a formulation for the bed slope effect that was developed for bed load transport only. Thus the total sediment transport is treated as if it were bed load. Since suspended transport forms generally the majority of the total transport in tidal embayments, the bed slope effect is thus somewhat overestimated.

[17] The adjustment of sediment transport for bed slope effects is executed into two steps. First, the magnitude of the sediment transport vector is adjusted in case of a bed slope in the same direction as the initial sediment transport vector, defined here as the longitudinal direction (s). It is noted that in the current model the initial sediment transport vector has the same direction as the depth averaged flow velocity vector. The size of the adjustment is calculated following a modified form of the expression suggested by *Bagnold* [1966]:

$$\overrightarrow{S'} = \alpha_s \overrightarrow{S} \tag{6}$$

where

$$\alpha_s = 1 + \alpha_{bs}\left[\frac{\tan(\phi)}{\cos\left(\tan^{-1}\left(\frac{\partial z_b}{\partial s}\right)\right)\left(\tan(\phi) - \frac{\partial z_b}{\partial s}\right)} - 1\right] \tag{7}$$

$\overrightarrow{S}$ initial sediment transport vector, $m^3/m/s$;
$\overrightarrow{S'}$ adjusted sediment transport vector, $m^3/m/s$;
α_{bs} coefficient with default value of 1;
ϕ internal angle of friction of bed material (assumed to be 30°), deg;
$\frac{\partial z_b}{\partial s}$ bed slope in longitudinal direction;
and

$$\left(\frac{\partial z_b}{\partial s}\right)_{\max} = 0.9\tan^{-1}(\phi). \tag{8}$$

[18] Secondly, the direction of the bed slope transport vector is adjusted for a bed slope in the direction normal to the initial sediment transport vector, referred to as (n). This is done by calculating an additional sediment transport vector perpendicular to the initial sediment transport vector. The magnitude of this vector is calculated using a formulation based on the work of *Ikeda* [1982] as presented by *Van Rijn* [1993]:

$$S_n = \left|\overrightarrow{S'}\right| \alpha_{bn} \frac{u_{cr}}{\left|\overrightarrow{u}\right|} \frac{\partial z_b}{\partial n} \tag{9}$$

where

S_n magnitude of additional sediment transport vector. The direction of this vector is downslope, $m^3/m/s$;
α_{bn} coefficient, default value = 1.5;
u_{cr} critical (threshold) depth-averaged flow velocity, m/s;
$\overrightarrow{u}$ depth-averaged flow velocity vector, m/s;
$\frac{\partial z_b}{\partial n}$ bed slope in the direction normal to the initial sediment transport vector.

[19] The resulting sediment transport vector ($\overrightarrow{S_r}$), which is adjusted for magnitude and direction, is calculated by:

$$\overrightarrow{S_r} = \overrightarrow{S'} + \overrightarrow{S_n} \tag{10}$$

2.2.3. Bed Level Update

[20] Conservation of sediment is described by the following equation representing a balance between the divergence of the sediment transport field and the evolution of the bed level corrected for bed porosity:

$$(1-\varepsilon)\frac{\partial z_b}{\partial t} + \frac{\partial S_x}{\partial x} + \frac{\partial S_y}{\partial y} = 0 \tag{11}$$

where

ε bed porosity, default 0.4;
z_b bed level, m;
S_x sediment transport in x direction, $m^3/m/s$;
S_y sediment transport in y direction, $m^3/m/s$.

[21] Following equation (11) the bed level in the model is updated every time step on the basis of a constant porosity and sediment transport gradients along a grid cell.

2.3. Geometry and Configuration

[22] The configuration of the model is highly schematized and consists of a rectangular box that has an open boundary at the seaward end, see Figure 2. Thus no flow or transport is allowed across the sides and at the landward end. At these locations a no-slip condition applies. The reason why a rectangular configuration was chosen is twofold. First, it makes comparison possible with earlier research carried out by *Schuttelaars and De Swart* [1996, 1999, 2000], *Seminara and Tubino* [2001], *Schramkowski et al.* [2002, 2004] and *Hibma et al.* [2003b] who all used rectangular basins or assumed that no significant changes of the basin width occurred over a typical length scale of the developing bars. The second reason is that a basin with an exponentially varying width or a real geometry would complicate the analysis of model results, especially concerning the hydrodynamic behavior.

[23] The length (L) of the embayment for the 2-D schematization is 80 km and the width (W) has a value of

2.5 km. This size was chosen because it somewhat resembles the size of the Western Scheldt estuary in the Netherlands so that comparison to measured data would be possible, see Figure 1. The Western Scheldt is particularly suitable for comparison with this model since river discharges are very small compared with the tidal prism (<1%), so that the morphodynamics are tide dominated. The current model deviates from the model described by *Hibma et al.* [2003b] in the sense that erosion of dry cells is allowed, that the ''online'' approach is applied with a fixed morphological factor instead of tidal residual transports with a MF depending on courant conditions, that a different formulation of the bed slope effect is applied and that longer runs are made (i.e., 800 years instead of 120 years).

[24] In order to investigate the sensitivity of the model to different basin lengths and widths, additional 2-D runs were performed for a length of 20 km and widths of 1.25 km and 5 km. It is noted that 20 km basins correspond to a short basin having a length that is small compared to the tidal wavelength. The 80 km basins approach values of $^1/_4$ of the tidal wavelength. This induces resonance resulting in observed increasing amplitude (up to 5 m.) toward the head.

[25] The grid size of the 1-D model schematization is uniform and 62.5 m (lateral) × 125 m (longitudinal) in size. The grid size of the 2-D model is uniform and is 62.5 m (lateral) × 125 m (longitudinal) m thus allowing a detailed description of the growth of bars that are typically 1–2 orders of magnitude larger than the grid size. The boundary at the seaward end is defined by a varying water level with amplitude (A) of 1.75 m and a period (T) of 12 h slightly deviating by 42 min from the M_2 tidal period. The sediment transport at this boundary was defined by an equilibrium transport corresponding to the value of the velocities at the boundary. The boundary thus allows for net sediment fluxes over a tide. The grain size of the sediment is uniform and has a value (D) of 240 μm. Courant conditions required a hydrodynamic time step of approximately 1 min. The used value of Manning's coefficient was 0.026 $sm^{-1/3}$. The value of the eddy viscosity, ν_e, was 0.1 m^2/s. Standard value for bed slope factor α_{bn} was set to 5. Although *Ikeda* [1982] suggests a value of 1.5 based on small-scale experiments, this leads to unrealistic channel profiles.

2.4. Numerical Aspects

2.4.1. Hydrodynamics

[26] The numerical scheme applies an orthogonal, staggered grid, where water level points and depth points are colocated in the cell centers and the u and v velocity points are located in the middle of the cell walls. An Alternating Direction Implicit (ADI) method is used to solve the continuity and momentum equations [*Leendertse*, 1987]. The advantage of the ADI method is that the implicitly integrated water levels and velocities are coupled along grid lines leading to systems of equations with a small bandwidth. *Stelling* [1984] extended the ADI method of Leendertse with a special approach for the horizontal advection terms, namely the splitting of a third-order upwind finite difference scheme for the first derivative into two second-order consistent discretizations: a central discretization and an upwind discretization, which are successfully used in both stages of the ADI scheme. The scheme is denoted as the ''cyclic method'' [*Stelling and Leendertse*, 1991].

2.4.2. Morphodynamics

[27] With respect to the bed slope effects on the sediment transport described in section 2.2.2, the longitudinal and normal bed slopes are calculated by

$$\frac{\partial z_b}{\partial s} = \frac{\partial z_{(u)}}{\partial x}\frac{S_x}{\left|\vec{S}\right|} + \frac{\partial z_{(v)}}{\partial y}\frac{S_y}{\left|\vec{S}\right|} \tag{12}$$

$$\frac{\partial z_b}{\partial n} = \frac{\partial z_{(u)}}{\partial x}\frac{S_y}{\left|\vec{S}\right|} + \frac{\partial z_{(v)}}{\partial y}\frac{S_x}{\left|\vec{S}\right|} \tag{13}$$

where $\frac{\partial z_{(u)}}{\partial x}$ is bed slope in the positive x direction evaluated at the U point; $\frac{\partial z_{(v)}}{\partial y}$ is bed slope in the positive y direction evaluated at the V point; and $\vec{S}$, S_x, S_y is the initial sediment transport vector, the initial sediment transport in x and y direction, respectively, $m^3/m/s$.

[28] With respect to the morphodynamic model the following important procedures, slightly deviating from *Lesser et al.* [2004], were followed: (1) The depths in u and v points are taken as the minimum of the surrounding depths in water level points; (2) the velocity vectors applied in the centers are determined by a depth-weighted averaging of the surrounding velocities in u and v points; (3) the sediment transport components in the u and v points are copied from the upstream water level points where the bed load transport is evaluated; and (4) the bottom change (in water level points) over half a time step is computed as the net sediment transport into or out of a cell, multiplied by the morphological factor.

[29] It is stressed that bed level changes at the mouth boundary may take place for outgoing (seaward) flow. In contrast, no bed level changes are allowed for ingoing (flood) flow at the mouth boundary cells.

2.4.3. Morphodynamic Update

[30] Tidal hydrodynamic behavior in estuaries has a timescale that is typically 1 to 2 orders of magnitude smaller than the morphodynamic timescale [*Wang et al.*, 1991]. In terms of numerical modeling this implies that many hydrodynamic calculations need to be performed that have only limited effect on the morphology. It is only after several weeks that the impact on the bed becomes relevant. Morphodynamic calculations would therefore require long and inefficient hydrodynamic calculation time. In order to increase the efficiency of process-based morphodynamic models different techniques have been developed. For example, *Latteux* [1995] describes, among others, the concept of the morphological tide that uses the residual sediment transport calculated over one tide to update the bed for a next hydrodynamic calculation. *Roelvink* [2006] compares a tide averaging method with continuity correction (RAM) to the ''online'' method and concludes that the ''online'' approach is most favorable. In this approach the bed level change calculated every hydrodynamic time step is increased by a morphological factor and results in the bed level used in the next hydrodynamic time step. Model

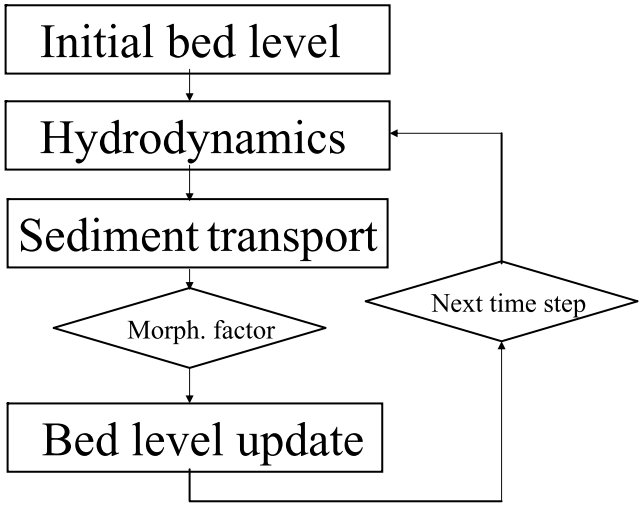

Figure 3. Morphological update scheme.

results are valid as long as bed level changes after a time step remain small compared to the water depth. The update scheme is presented in Figure 3. Main advantage is that the stability and accuracy of the method are less restrictive than for the tidally averaged method (RAM) and that it allows propagation of morphological features during a tide.

[31] In our model the ''online'' approach is applied with a morphological factor (MF) of 400. The sensitivity tests carried out by *Roelvink* [2006] are based on tidal inlet geometry somewhat differing from the current research geometry. It is, however, expected that the allowed value of the morphological factor will depend on the modeled processes (i.e., waves and/or tides) and model configuration, so that its final value needs to be determined per case. The results of an extensive sensitivity analysis of different values of the MF are discussed more closely for the 1-D configuration in section 3.1 and for the 2-D configuration in section 4.6.

2.4.4. Drying and Flooding

[32] The intertidal area in the model falls dry and becomes wet during the tidal cycle. Therefore a proper description of the drying and flooding procedure is needed. *Bates and Hervouet* [1999] provide a review of techniques on the matter and *Lanzoni and Seminara* [2002] used the work of *Defina* [2000] in their model. This approach is based on a statistical description regarding sub grid bed level variations of shallow cells including the effect of advection and friction.

[33] The current research applies the method described by *Hibma et al.* [2003b, 2003c] in which the cells that fall dry are removed from the hydrodynamic calculation. When the tide rises and the cells become wet again, they are reactivated. Cells become dry when the water depth decreases below a certain threshold value (0.1 m in this study). This means that the velocity is set to zero. The cell is closed at the side normal to the velocity. When all four velocity points of a cell surrounding a water level point are dry, the cell is excluded from computation. If the water level rises and becomes larger than twice the threshold level (2 * 0.1 m in this study), the velocity point is reactivated.

2.4.5. Dry Cell Erosion

[34] The advantage of using a morphological factor is that it accelerates the morphodynamic calculations in such a way that the computational effort can be drastically decreased. The disadvantage of high values of the morphological factor is that it may lead to a wrong description of the physical processes, because erosion and deposition processes are extrapolated. At certain locations and instances this may even result in a water depth below the threshold value for wet cells described in the previous section or in a bed level, which exceeds high water. These cells are defined to become dry. The cells with bed levels exceeding high water even develop into fixed points that cannot participate in the erosion processes anymore and undermine the morphodynamic character. The problem is not only apparent for the ''online'' approach, but holds for all methods that apply an accelerated bed level update. For example, *Hibma et al.* [2003b] experienced the development of fixed points at the shoals using a similar configuration as the current research only with bed level updates based on tidally averaged transports.

[35] The problem is overcome by allowing erosion of dry cells in such a way that the erosion that is taking place in a wet cell is assigned to the adjacent dry cell. Implicitly this means that sediment is transported from a dry cell to a wet cell so that no bed level change of the wet cell takes place. The procedure continues until the dry cell becomes wet again. The procedure is not solely applied to cells with a bed level exceeding the highest water level during the tide but also for cells becoming dry during the tidal cycle. The procedure is more extensively described and applied by *Roelvink et al.* [2003].

[36] The following example of intertidal area becoming dry during the tide may illustrate the combined processes of drying and flooding and dry cell erosion. Assume a falling tide which results in a particular cell becoming dry when the water depth becomes lower than 0.1 m. No erosion of the cell can take place anymore because of transport processes within the cell. However, erosion may take place when the adjacent wet cell erodes. This erosion is attributed to the dry cell, which may become wet again when its water depth exceeds 2 * 0.1 m. The erosion of the dry cell should then be considered as resulting from bank erosion effects at the boundary between the wet and the dry cell rather than from erosion by hydrodynamic processes within the dry cell.

3. Model Results

3.1. One-Dimensional Schematization

[37] In the following section profile evolution will be investigated using a 1-D approach. The assumed existence of equilibrium profiles will be addressed as well as the governing processes that determine the profiles. The outcomes will be used to act later as initial conditions for the 2-D schematization.

[38] One-dimensional model runs were carried out using the same settings as for the 2-D model. Figure 4a shows the profile evolution starting from an initially horizontal bed level at 10 m-MSL (Mean Sea Level) along an 80 km long

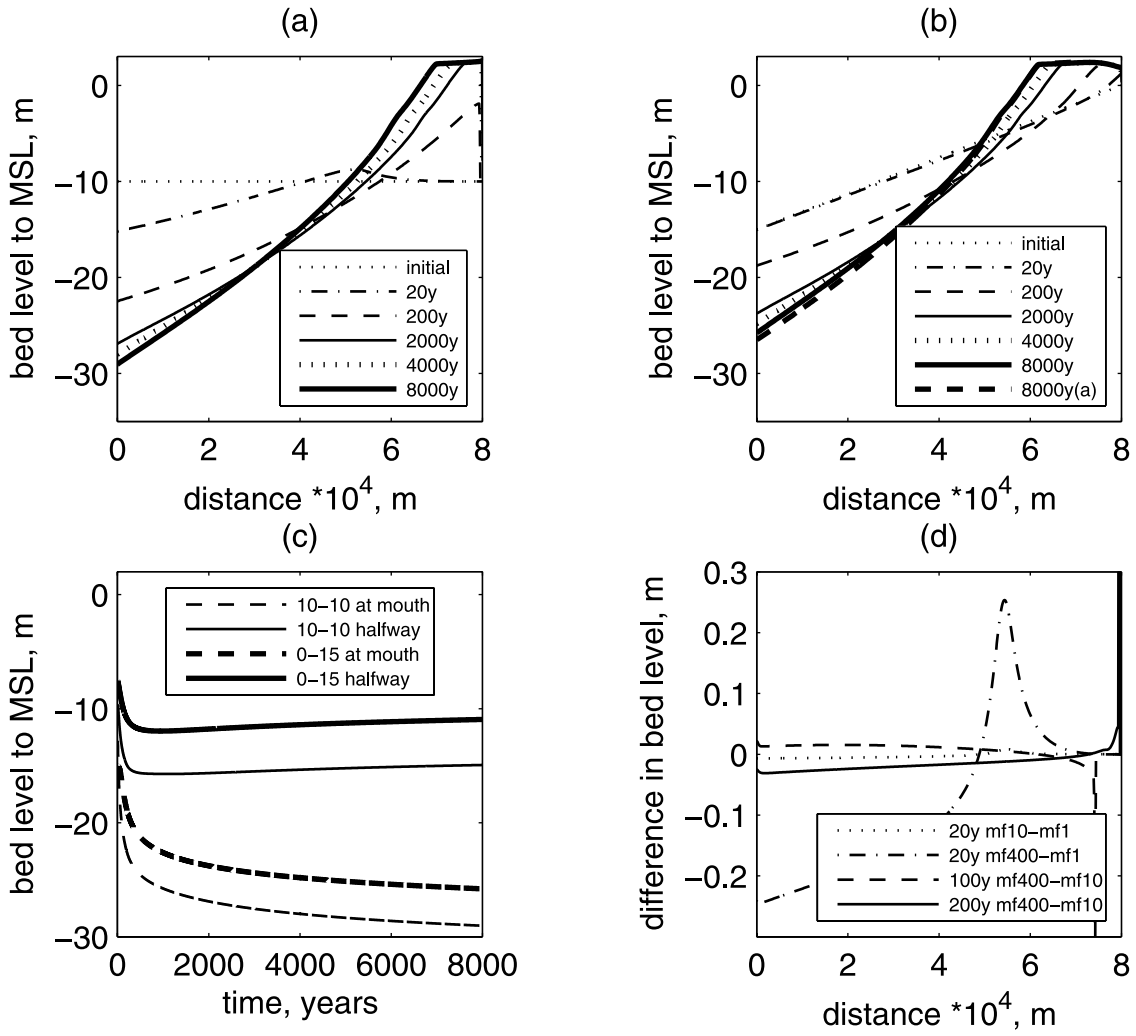

Figure 4. One-dimensional model results: (a) profile evolution from horizontal flat bed at 10 m-MSL, (b) profile evolution from linearly sloping bed from 15-MSL to MSL, (c) bed level development over time at mouth and halfway the basin for the different initial conditions, and (d) differences in bed level for different morphological factors at different points in time.

basin. Halfway the basin a front migrates toward the head, whereas at the same time the bed level more seaward deepens considerably. After 8000 years the model results show a profile sloping from about 30 m-MSL at the mouth toward approximately 2 m + MSL near the head. Sedimentation takes place near the head although this takes place at a decreasingly smaller rate. Figure 4b shows similar profile evolution from a different and more shallow initial profile, i.e., sloping from 15 m-MSL at the mouth toward MSL at the head.

[39] After 8000 years both profiles are approximately similar apart from the seaward shift for the shallow profile that shows more sedimentation near the head. Figure 4b includes the profile of Figure 4a fit by a sea ward shift. The higher sedimentation rates in case of the shallow initial profile are attributed to the shallowness of the basin. The shallower a basin becomes, the more ebb flows and ebb wave propagation are hampered so that ebb duration increases. This leads to smaller flood duration, higher flood velocities and more sediment being transported landward during flood. Figure 4c shows that even after 8000 years no equilibrium was found in terms of a constant bed level at the mouth and halfway the basin, although evolution shows strongly asymptotic behavior.

[40] Figure 4d shows the results of a sensitivity analysis carried out for different values of the MF (i.e., 1, 10 and 400 after 20 years and 10 and 400 after 100 and 200 years) for different points in time for the basin with the horizontal bed at 10 m-MSL. The analysis shows that different values for the MF result in similar behavior of the profile with only (very) small differences even on the longer term. The pronounced peaks in the Figure 4d especially at 100 and 200 years are related to the local and temporal conditions of the steep front of the bed migrating toward the head. Bed level differences for different MFs reduce again when the steep front passes along. Sensitivity analysis was also carried out using a 2000 years bed level generated by a MF of 400 as initial bed and applying different values for the MF (i.e., 1 and 400, not shown). This showed even smaller differences than starting from a linear or horizontal bed.

Table 1. Overview of Morphological Duration in Years for Different Model Runs

	Length, km		
Width, km	20, Short	80, Long, Deep	80, Long, Shallow
1.25 narrow	1600	800	800
2.5 standard	1600	800	800
5 wide	800	none	400

[41] Various researchers investigated 1-D profile evolution in a tidal embayment using a model description similar to the current approach, i.e., water motion by the depth integrated shallow water equations in combination with a sediment transport formulation. *Van Dongeren and De Vriend* [1994] and *Schuttelaars and De Swart* [1996, 2000] found a linearly sloping bed level for a basin that is short compared to the tidal wavelength (just like in the current research), despite the fact that they used slightly different formulations for the sediment transport. Both imposed a zero sediment transport at the head. *Schuttelaars and De Swart* [1996, 2000] based their equilibrium profiles on the criterion of vanishing tidally averaged transports, which excluded the process of drying and flooding during the tide. *Van Dongeren and De Vriend* [1994] argue that the evolution toward the equilibrium is not obvious, because the boundary condition of zero sediment transport at the head would lead to continuous sedimentation and the creation of intertidal area at the head, especially when conditions are considered that are not tidally averaged. Equilibrium would finally develop in a balance between the basins' infilling capacity and the exporting effect due to the creation of intertidal area. The latter effect is extensively described by *Friedrichs and Aubrey* [1988] and is caused by the fact that intertidal area hampers the propagation of the flood wave, so that the flood period is elongated and ebb velocities and sediment export increase.

[42] *Lanzoni and Seminara* [2002] included a formulation for wetting and drying of intertidal area and solved the set of shallow water equations in a similar numerical approach as in the current research, although they assumed a different basin geometry with a landward exponentially decaying shape, included both bed load and suspended load transport, applied a different description for drying and flooding and did not extend their duration more than 300 years. Their results (for a 30 km basin) show a concave profile with asymptotically vanishing tide-residual sediment transports and the continuous formation of intertidal area near the head. It would be expected that longer model runs would reveal the formation of more intertidal area near the head, similar to the current 1-D model outcomes.

[43] The short literature overview indicates that a proper formulation of the boundary including drying and flooding of cells at the head is essential. The current model applies an approach that includes drying and flooding of the intertidal area developing near the head. The results show a continuous sedimentation at the head. Furthermore, shallower initial conditions will lead to more sedimentation. The sedimentation process only decreases because the deepening of the more seaward located profile leads to lower transport rates toward the head. The shape of the evolving profile remains similar for different initial conditions. This supports the suggestion that the profiles after 8000 years are close to equilibrium.

3.2. Two-Dimensional Schematization

[44] Two-dimensional long-term calculations (up to 4 years of hydrodynamic calculations with an equivalent of 1600 years of morphodynamic development) were carried out in order to investigate the evolution of the specific model configurations. Since computational effort took typically 2 weeks per run, only 8 runs are elaborated in this article. These configurations are given in Table 1. In the following sections the model results are analyzed. Animation 1[1] shows an example of 800 years of morphodynamic evolution.

[45] The authors used an approximation of the 8000 years 1-D profiles as a basis for the initial bed level for further research. The reason was that preliminary 2-D calculations showed that long run durations ($\sim$2 weeks) were needed to allow for patterns to develop toward dynamically stable shapes. This urged the authors to find 2-D initial conditions close to eventual equilibrium profiles. The profiles were linearized starting from MSL at the head to 8 m-MSL for the short basin and 34 m-MSL for the long basin. However, preliminary calculations showed (see section 3) that patterns hardly developed in this long basin. Therefore, and because width-averaged bed levels in the Western Scheldt estuary are typically in the order of 10–15 m-MSL, the initial 2-D bed level was taken as linearly varying from 15 m-MSL at the mouth to MSL at the head, which is referred to as the long, shallow basin. For all 2-D configurations the initial bed was disturbed randomly with values of maximum 5% of the local water depth in order to trigger channel and shoal development.

3.2.1. Pattern Formation

[46] Figure 5 presents an overview of the pattern formation after 15, 100 and 800 years for a 2.5 km wide, long, shallow basin. Also, Animation 1 shows 800 years of morphodynamic evolution for the 2.5 wide and 80 km long basin. Initially the model shows major bar growth in the relatively shallow part near the head including relatively small bars. *Seminara and Tubino* [2001], *Schuttelaars and De Swart* [1999], *Schramkowski et al.* [2002] and *Dronkers* [2005] extensively describe the prevailing processes in bar development for the linear domain where the bars themselves do not yet significantly influence the velocity field. Local tidal velocities and bed slope effects on the sediment transport govern the dominant length scale of these bars and their growth rates.

[47] Later on and more seaward a front of the channel-shoal pattern develops toward the deeper parts of the basin. The front does not originate from instabilities caused by local tidal velocities like in the more shallow parts of the estuary, but it emerges from high ebb velocities elongating the channels while bars develop at the seaward end of these channels. Finally, some crests of the bars enter the intertidal domain, which makes them less subject to hydrodynamic processes. Although migration, growth and erosion are still going on, the bar position and shape become less dynamic. Seaward bar migration still takes place after 100 years, but the migration rate decreases exponentially with time. It

[1] Animation 1 is available in the HTML.

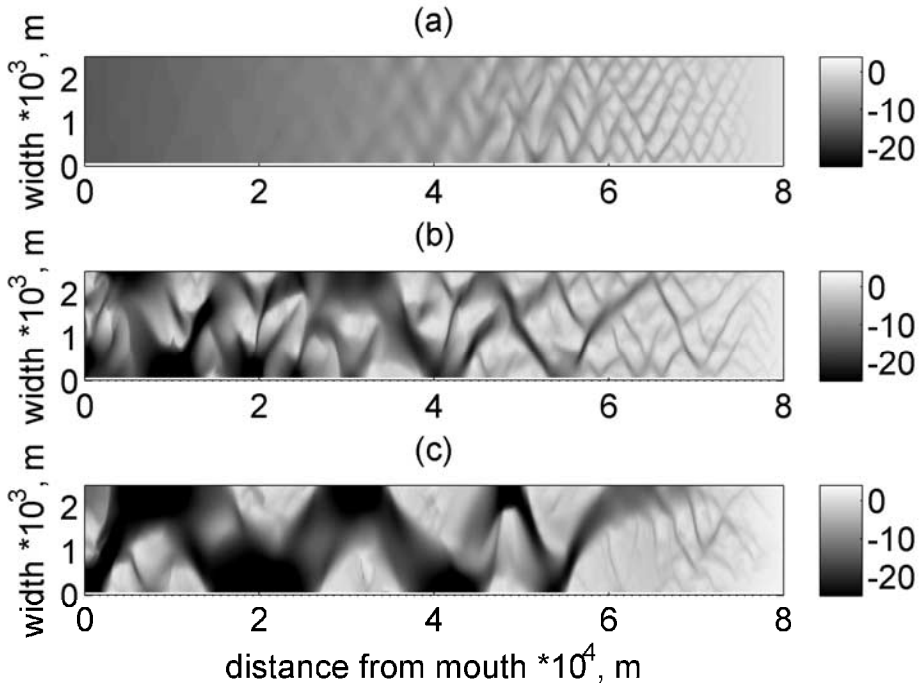

Figure 5. Pattern formation for the shallow basin in m (2.5 km wide and 80 km long), (a) after 15 years, (b) after 100 years, and (c) after 800 years. Not on scale.

becomes probably finally related to the (slow) adaptation rate of the longitudinal profile. Figure 6 shows results after 800 years for both the short basin and the long shallow basin with varying widths. It can be clearly seen that relatively long and narrow basins generate an alternating bar pattern separated by a sine-shaped channel. Near the mouth the alternate bars are subtidal, but more landward the bars have crests in the intertidal and supratidal domain. Still after 800 years these bars have a tendency to migrate seaward, with a typical rate of 1 km/100 year. The meandering channel significantly deepens at the sides of the basin. Occasionally, the channel includes the characteristics of a combined ebb and flood channel separated by a small shoal in between. The wider the channel bed, the more it becomes subject to distortions, and bar development. It is believed that in case of wider basins the sine-shaped channel becomes so wide that the bars in the channel disturb the channel hydrodynamics in such a way that a dynamic multiple channel system will develop.

[48] The pattern of relatively short and wide basins is more determined by free behavior of the bars in the sense that their development seems not restricted by the banks of the embayment. After 800 years the channels keep showing a meandering behavior and no single channel dominates the pattern formation. This also holds for the shallower parts of relatively narrow basins near the head.

[49] The long deep basin (not shown in Figure 6) shows similar behavior, although intertidal area only develops near the head and the front of the pattern formation does not reach the mouth, not even after 1600 years.

[50] On the basis of a 2-D model *Schramkowski et al.* [2004] extend their work of 2002 to the nonlinear regime and found conditions for static and dynamic (pulsing) morphodynamic equilibria of patterns. These equilibria were related to narrow (with a width small compared to the tidal excursion length) and relatively deep basins and refer to an alternating bar pattern also found in the current model. For wider and shallower basins, only time-dependent states could be found. This agrees well with the current model results.

3.2.2. Morphological Wavelength

[51] Model results show a range of characteristic bed forms. *Yalin and Da Silva* [1992] suggest a relationship between the spacing of the bars and the basin width in a situation of alternating bar forms based on an inventory of empirical research:

$$L_B = 6B \tag{14}$$

where L_B is length of bar spacing, m, and B is basin width, m.

[52] The relationship was derived and validated for relatively small values of the width to depth ratio (10 < width/depth < 100) and for fluvial conditions only.

[53] Contrary to equation (14) the model results suggest that a characteristic morphological length scale (defined as the characteristic morphological feature that can be observed) is not solely and linearly a function of the basin width. We suggest an equation which relates the morphological wavelength to the tidal excursion, the width-averaged depth and the basin width as follows:

$$L_{mw} = \delta \frac{\sqrt{\alpha_{bn}}}{c_f} \frac{\sqrt{B} E \overline{h}}{T\sqrt{g}} \tag{15}$$

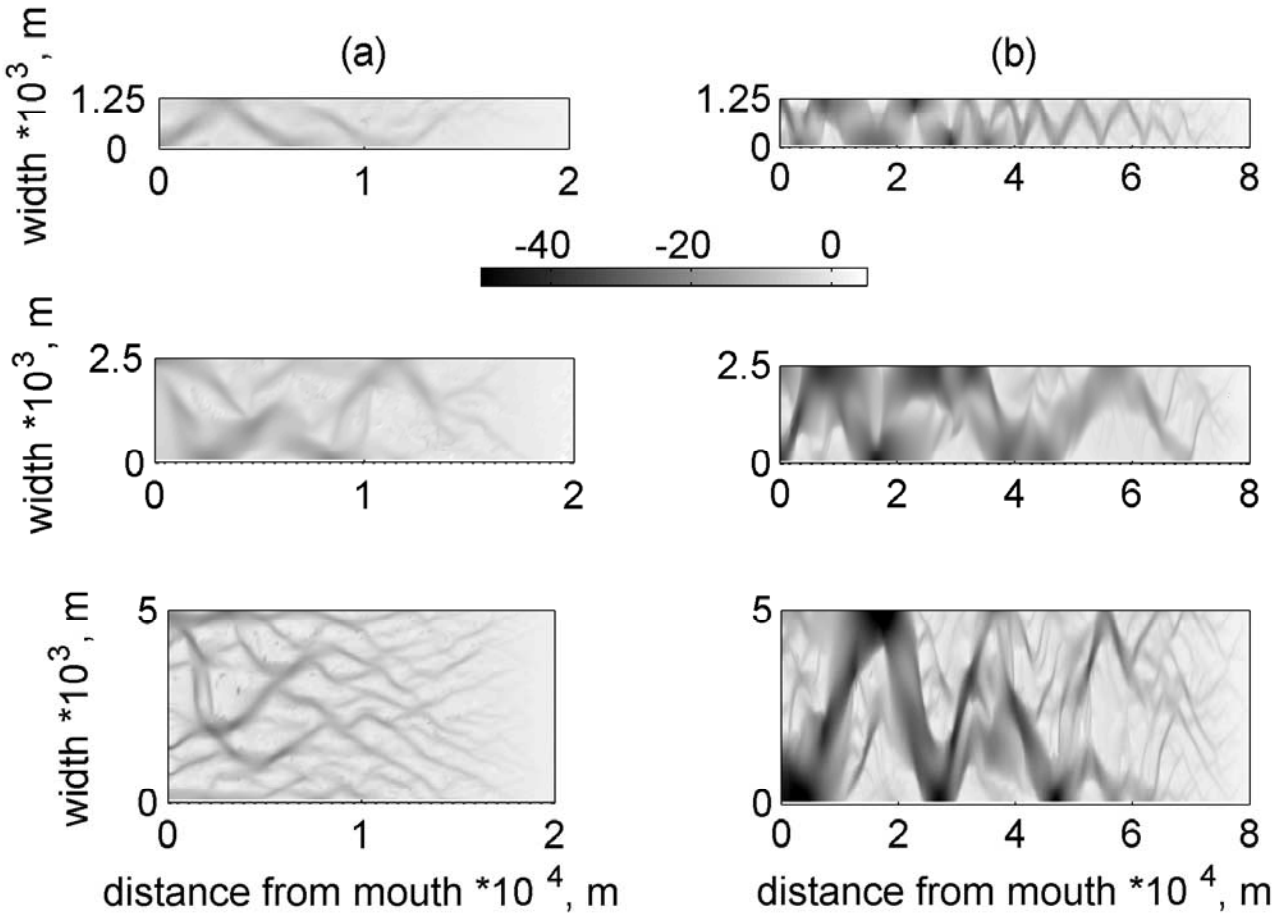

Figure 6. Not on scale. Pattern formation in m for (a) a 20 km long basin with varying widths (presented results after 1600, 400 and 400 years, respectively) and (b) a 80 km long, shallow basin with varying widths (presented results after 400, 1600 and 400 years, respectively).

or, in other terms,

$$L_{mw} = \delta \frac{\sqrt{\alpha_{bn}}}{c_f} \frac{P}{T\sqrt{Bg}} \tag{16}$$

where

L_{mw} morphological wavelength, m;
δ coefficient, m^{-1};
B basin width, m;
E tidal excursion defined by P/A, m;
P tidal prism (amount of water flowing through a cross section from Low Water Slack to High Water Slack at a certain location), m^3;
A minimum cross section below MSL, m^2;
$\bar{h}$ minimum width-averaged water level below MSL, defined by A/B, m;
T tidal period, s.

[54] The equation was derived by curve fitting and systematically varying the model parameters basin width (B), the tidal prism (P) and the minimum cross section below MSL (A). The tidal excursion (E) was defined by (P/A) and the mean water depth ($\bar{h}$) by (A/B), thus representing the minimum width-averaged water level below MSL. The model parameters were investigated for a root, linear and quadratic relationship (both in the nominator and the denominator) with the morphological wavelength.

[55] Figure 7b plots a comparison of model results observations and results from equation (16) for a value of 0.3 for (δ). For dominant alternate bar patterns, the morphological length scale was determined by multiplying the distance between a channel sinus "crest" and a "trough" by two. For dominant multichannel beds, the length of the bars was supposed to determine the morphological length scale. Data from the Western Scheldt resemble to the model results of the long basin only to some extent. This is attributed to the meandering shape the Western Scheldt itself has, see Figure 1, the presence of nonerodible layers as well as model idealizations like the formulation of sediment transport and bed slope effects. Section 4 will discuss the characteristics of equation (16) in more detail.

3.2.3. Longitudinal Profile

[56] For the short, 2.5 km wide basin, Figure 8a shows longitudinal profiles of the width-averaged bed level for different points in time. The initial, linear profile apparently does not fit the hydrodynamic conditions, since a more concave profile develops over time. At the head sediment settles slowly, although the rate seems to decrease expo-

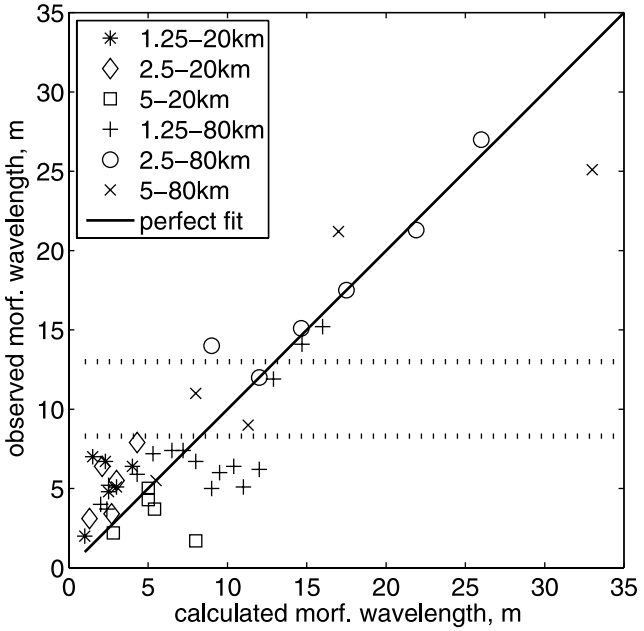

Figure 7. Morphological wavelength calculated by equation (16) versus the morphological wavelength observed in model results. Range of data from the Western Scheldt estuary is represented by the intercepted lines.

nentially with time. The 1-D model results, starting from the same initial bed level, show similar behavior although the profile does not show disturbances from pattern formation. Figure 8b shows comparative 2-D results for different widths of the basin. Results originating from a different randomly distributed initial bed (not shown) show a range of similar deviations of the profile near the mouth. In Figure 8c, the shallow, long basin shows an increasing deepening of the concave profile. It is remarkable that the bed level at the mouth holds the value of 15 m-MSL, although the bed levels in the basin itself continue to decrease. The 1-D model results show considerable sedimentation at the head which is even more pronounced than the results of the 2-D model (compare Figures 4b and 8c). The 2-D model transports the excess sediment mainly on intertidal shoals generated along the complete basin. This allows for less sedimentation near the head.

[57] Figure 8d shows results for the deep, long basin with only minor sedimentation at the head, because of the deeper initial profile. The front of the pattern formation toward the sea can still be recognized, indicating that this is still an ongoing process after 800 years. Apparently, the large depth decreases tide residual transports and increases the morphodynamic timescale significantly.

3.2.4. Cumulative Transports

[58] Figure 9 shows width-integrated cumulative sediment transports through different cross sections for the short and shallow, long basins, both 2.5 km wide. It is noted that the lines in Figure 9 show long-term behavior, whereas a look on a more detailed timescale would reveal tidal fluctuations of the sediment transport. It appears that the tide residual transports have their own, relatively large timescale, although they are smaller than typical transports during the tide. This is despite the application of the high (~400) morphological factor. This will be discussed more closely in section 4.

[59] Both basins show similar behavior. Near the head sediment accumulates over time, whereas sediment is exported toward the sea for the remaining part of the basins. The cumulative transports show highly unsteady behavior especially near the mouth where the transports are highest. The short basin tends to an equilibrium situation without any additional transport, whereas the shallow long basin shows an exporting tendency due to the surplus of sediment present. The deep long basin (not shown in Figure 9) does only export small quantities of residual sediment at the mouth.

3.2.5. Comparison to Empirical Relationships

[60] One of the possibilities to investigate a possible equilibrium in the model is to compare the results with empirically derived relationships. *O'Brien* [1969] derived an empirical relationship between minimum cross-sectional area and the tidal prism through the cross section. The tidal prism is defined as the amount of water flowing through a cross section between low water slack and high water slack. *Jarret* [1976] reanalyzed the data of O'Brien and added data published by other authors. Data were derived from 108 inlets on the U.S. Gulf coast, the U.S. Pacific coast and the U.S. Atlantic coast. The equation derived for basins that had two jetties at the mouth (for the prevention of sedimentation caused by long shore drift) reads as follows:

$$A = 7.490 * 10^{-4} * P^{0.86} \tag{17}$$

where A is cross-sectional area below MSL, m^2, and P is tidal prism, m^3.

[61] Jarret also derived a relationship for nonjettied or single jettied basins, but these relationships match the model results less. The assumed reason for this is that the two jettied basins more closely match the rectangular model basin, allowing no influence of wave induced sediment transport at the mouth.

[62] Figures 10a and 10b show a comparison of the model results and equation (17). With time, all basins evolve toward a line similar to the Jarret relation. However, all model results over predict the cross section with respect to equation (17). This is in line with observations that the model generates relative deep channels. The slope of the line (represented by the 0.86 coefficient in equation (17)) fits the short basins well and model results suggest a steeper slope for the long shallow basin. Both the impact of friction and the behavior of the tide could be held responsible for this. The short basin is short compared to the tidal wavelength, whereas the long basin will face more impact of friction and the basin length approaches a value of a quarter of the tidal wave which induces resonant behavior.

[63] Comparable to the investigations by O'Brien and Jarret, on the basis of empirical research, *Eysink* [1990] suggests a relation between a characteristic tidal volume and the volume that the channels hold as follows:

$$V_c = c_c P^{\beta} \tag{18}$$

where

V_c channel volume below MSL, m^3;
c_c empirical coefficient;
P tidal prism, m^3;
β empirical power coefficient.

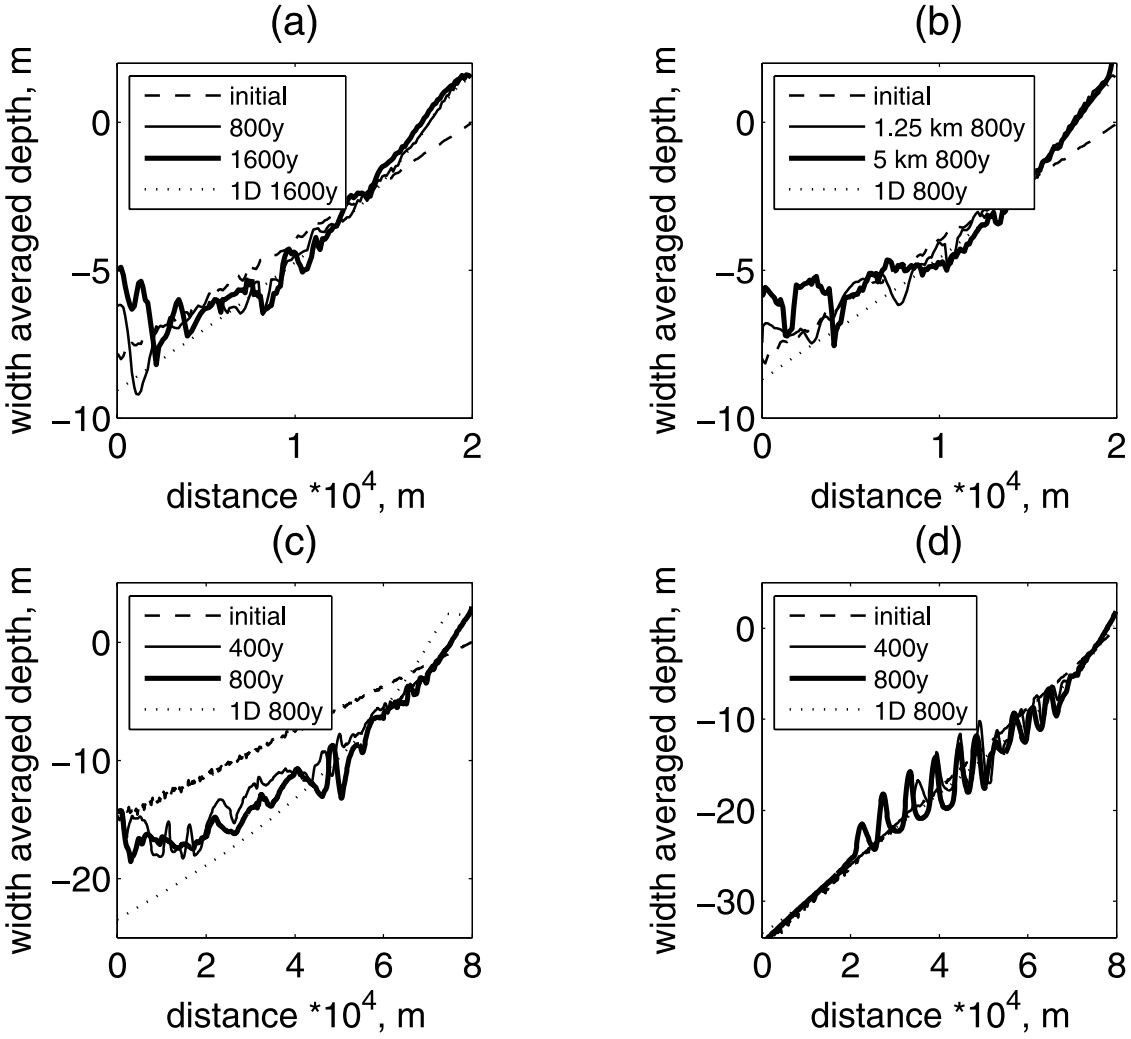

Figure 8. Longitudinal profile of the width-averaged depth (a) for different points in time for a short 2.5 km wide basin; (b) for short basin with different widths after 800 years of morphodynamic calculation; (c) for different points in time for the 2.5 km wide shallow, long basin; and (d) for different points in time for the 2.5 km wide deep, long basin.

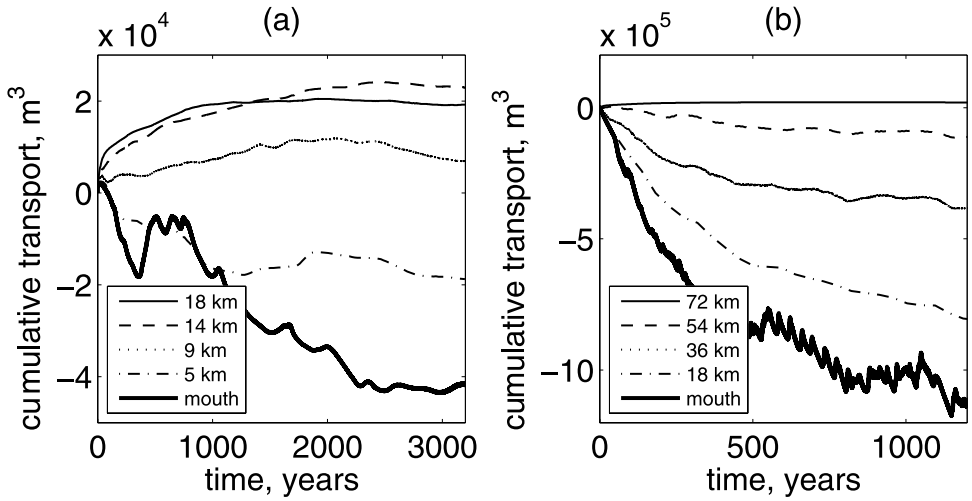

Figure 9. Width-integrated cumulative sediment transport in m^3 for 2.5 km wide basin for (a) short basin and (b) long, shallow basin.

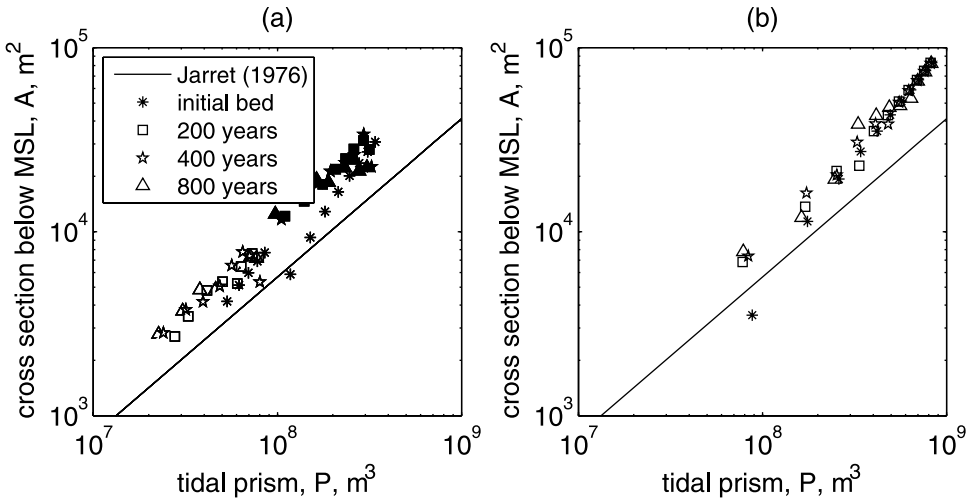

Figure 10. Relation between tidal prism (m^3) and the cross section below MSL (m^2) for different points in time. Per time point 7 to 8 locations in longitudinal direction (equidistance) are plotted on a logarithmic scale. The line represents the relation by *Jarret* [1976] for jettied inlets, see also equation (17). (a) Short, 1.25 km wide basin (open markers) and short 5 km wide basin (filled markers) and (b) long, shallow 2.5 km wide basin.

[64] For different basins in the Netherlands, Eysink calibrated the coefficient c_c to value ranging from 80 * 10^{-6} (Waddenzee, large intertidal area) to 65 * 10^{-6} (Western Scheldt, small intertidal area). β was kept constant at 1.5. Figure 11 shows a comparison of different model results, equation (18) (with c_c = 65 * 10^{-6} and β = 1.5) and measured values from *Eysink* [1990]. Development of the model results over time is only limited so that only end model results are plotted. Figure 11 shows that the basin width has an important impact on the model results. Relatively wide and short basins have a smaller channel volume (or larger intertidal area) for the same tidal prism. This is also apparent from Figure 5. Furthermore the model results show a steeper relationship than suggested by Eysink. For example, a best fit of equation (18) to the model results of an 80 km long 5 km wide basin resulted in a value of 10^{-8} for coefficient c_c and a value of 1.85 for β. This can be related to the fact that the model leads to a larger increase of intertidal area more landward. An explanation could be the neglect of waves eroding tidal flats (although this effect decreases more landward) or the absence of river discharge. Figure 11 also shows that the data from the Western Scheldt are comparable to a basin between 2.5 and 5 km wide, which is a typical width for both estuaries.

3.2.6. Hypsometry and Intertidal Area

[65] The hypsometric curve relates the basin surface area to the height above the deepest point of the basin. An expression describing the hypsometry for the intertidal area is given by *Boon* [1975]. However, no expression was found in literature describing the full hypsometry of a tidal embayment. Therefore we suggest the following power law

$$\frac{A_r}{A_{\max}} = \left(\frac{h_r}{h_{\max}}\right)^{\alpha} \tag{19}$$

where

A_r basin area at certain height above minimum depth, m^2;
A_{max} area at maximum depth, m^2;
h_r height above minimum depth, m;
h_{max} maximum depth, m;
α coefficient.

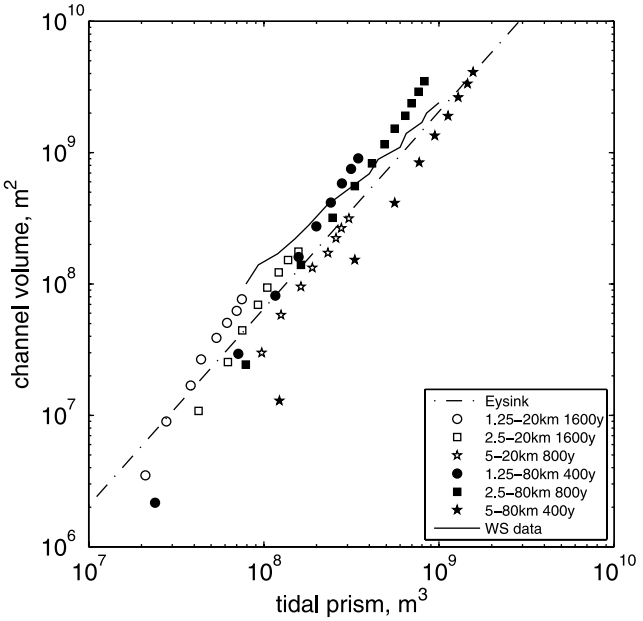

Figure 11. Relation between channel volume below MSL and tidal prism. Solid markers represent the short basin for different widths; open markers denote the long shallow basins. Comparison is made to measured values of the Western Scheldt [from *Eysink*, 1990]. The Eysink relation (equation (18)) is also shown.

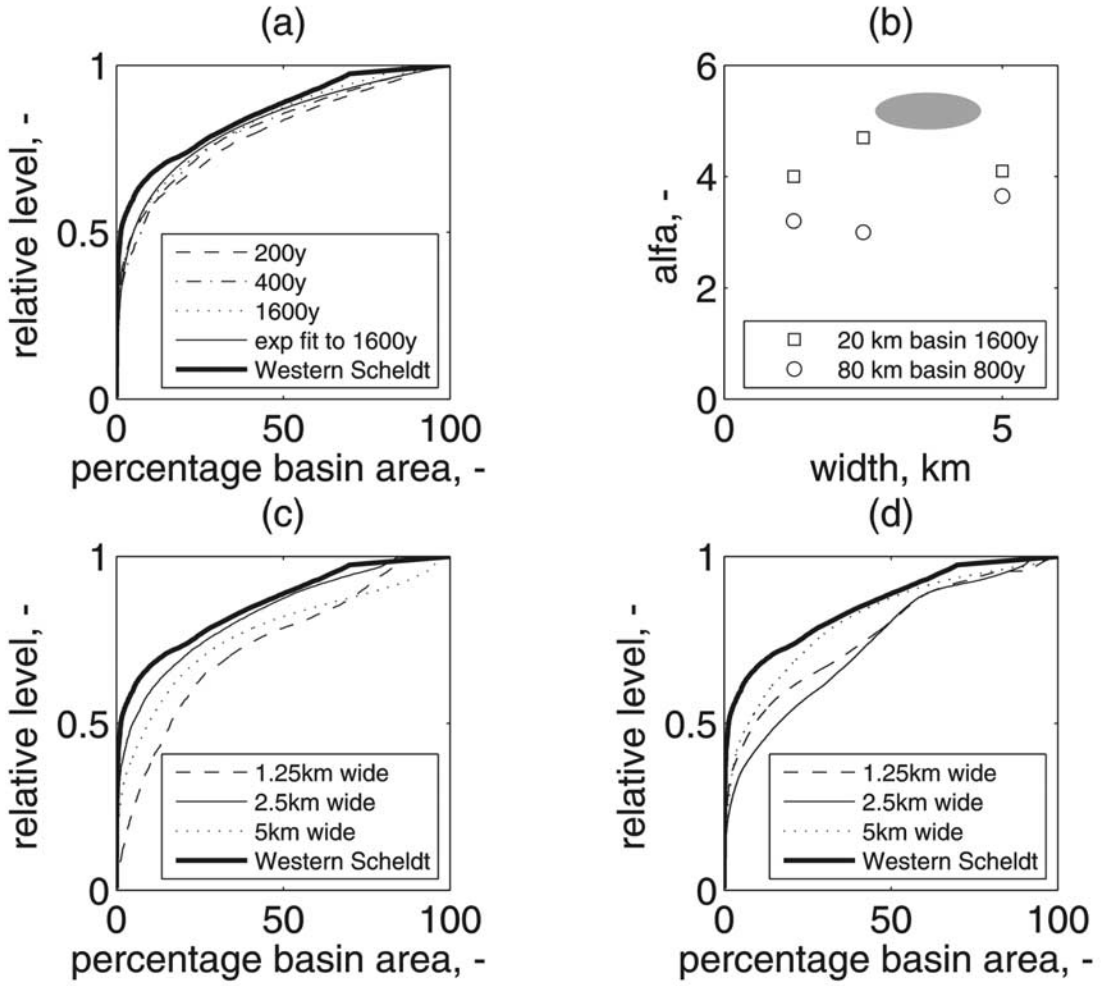

Figure 12. (a) Hypsometry for different points in time for a short basin, 2.5 km wide; (b) α values for different widths and short and long shallow basin; (c) hypsometry of short basin after 1600 years for different widths; and (d) hypsometry of long shallow basin after 800 years for different widths. For Figures 12a, 12c, and 12d, Western Scheldt data are bold. For Figure 12b, WS data are represented by the shaded area.

[66] Figure 12a shows the development of the hypsometry for four points in time and an exponential fit by equation (19) for a short basin. No major change of the hypsometric curve takes place over time suggesting that a certain type of equilibrium is present. Figures 12c and 12d show the hypsometry for different widths for the short (after 1600 years) and long (after 800 years) basin. The short basin shows a more convex profile than the long basin. Convex hypsometry is associated with relatively deep channels covering a relatively small area of the basin. Figure 12b presents an overview of the values for α for different sizes of the basin. It shows that the short basins are more convex than the long basins although this difference reduces for larger widths. Although the time period for the short basin is twice the time period of the longer basin, this does not significantly change the value of "α" considering the fact that the curves do not deviate much in time (see Figure 12a). Comparing model results by data from the Western Scheldt in Figure 12 shows that the latter is more convex than the model results.

[67] Results of the percentage of intertidal area compared to the basin area at high water are shown in Figure 13. It can be seen that the short basins show larger percentages of intertidal area. This corresponds to the more convex hypsometries that are associated with relatively deep channels covering a relatively small basin area. In addition, Figure 13 shows that the amount of intertidal area is rising with time (except in case of a 5–80 km basin) and that there is no indication for an asymptotic behavior toward equilibrium. This can be associated with the continuing sedimentation at the head, see also Figure 8. Furthermore it can be concluded from Figure 13 that the percentage of intertidal area is rising with increasing basin width, although this effect is less pronounced in case of longer calculation periods. The long deep basin has considerably less intertidal area. Data for the Western Scheldt (with a width ranging from 3 to 5 km in the first 50 km from the mouth) indicate values between the deep and the shallow long basins.

3.2.7. Ebb and Flood Dominance

[68] In the following section the effect of tidal distortion on flood or ebb dominance and the morphodynamic process will be elaborated.

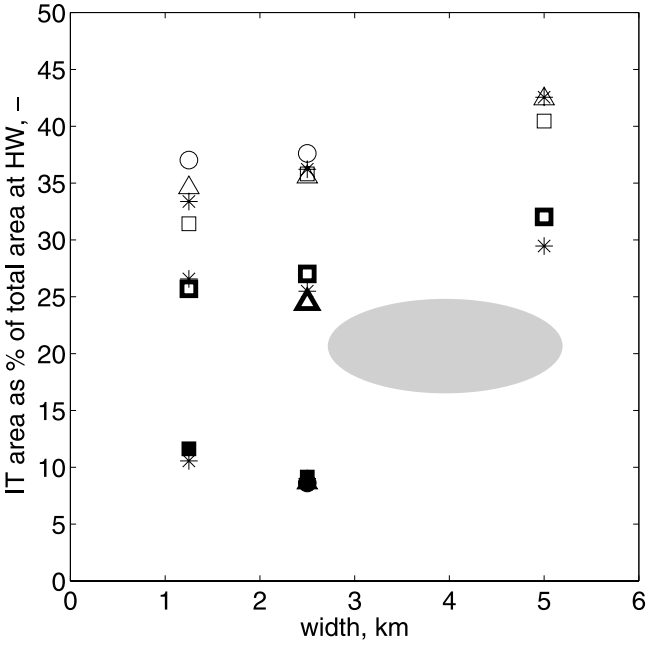

Figure 13. Relation between basin width and % of intertidal area with respect to the area at high water. Open markers represent the short basin, shaded markers represent the long, shallow basin and solid markers represent the long deep basin. Square denotes 200 year, asterisk denotes 400 year, triangle denotes 800 year, and circle denotes 1600 year. The shaded area shows a range of values found for the Western Scheldt over the last decade for the first 50 km. These values are not directly related to a width.

[69] On the basis of a 1-D model, *Speer and Aubrey* [1985] distinguished two important parameters with respect to ebb or flood dominance, namely the ratio of the volume of intertidal storage and the channel volume at MSL (Vs/Vc) and the ratio of the tidal amplitude and the mean water depth (A/h). Increasing values of the latter will elongate ebb duration with respect to flood duration, because of friction and because of the difference in wave propagation (where high water propagates faster than low water), which will both elongate ebb duration. Increasing values of intertidal storage will decrease flood propagation and thus elongate flood duration. *Friedrichs and Aubrey* [1988] confirmed the model results based on measurements along the U.S. Atlantic coast and used the model by Speer to come to predictions for ebb or flood dominance in case of adaptation of the tidal wave due to sea level rise [*Friedrichs et al.*, 1990].

[70] *Dronkers* [1998] assumed that equilibrium of the longitudinal bed profile would be present considering that the duration of flood equals the duration of ebb. An analysis based on the Saint Venant's equations results in the following expression

$$\left(\frac{h+a}{h-a}\right)^2 = \frac{S_{HW}}{S_{LW}} \tag{20}$$

with

h width-averaged water depth, (m);
a width-averaged tidal amplitude (m);
S_{HW} basin area at high water, (m^2);
S_{LW} basin area at low water, (m^2).

[71] *Wang et al.* [1999] investigated the consequences of the assumption made in equation (20) for the model by *Speer and Aubrey* [1985], by substituting their schematization into equation (20). The results are given here:

$$\frac{V_s}{V_c} = \frac{8}{3}\frac{\left(\frac{a}{h}\right)^2}{1-\frac{a}{h}}\left(\frac{1+\frac{a}{h}}{1-\frac{a}{h}}\right)\left(\frac{3}{4}+\frac{1}{4}\frac{a}{h}\right)^{-1} \tag{21}$$

[72] The equation describes a curve resembling the result of the model by *Friedrichs and Aubrey* [1988] and is used here mainly as an indication for flood and ebb dominance. It is stressed that Friedrichs and Aubrey used a highly schematized cross section differing from the current model, assuming, among others, a fixed ratio between the channel width and the depth (value = 120), a fixed geometry in longitudinal direction, a constant offshore forcing of 0.75 m and a fixed length of 7 km (which means that it is relatively short basin, contrary to the basin of the current model).

[73] Figure 14 plots equation (21) and the current model results developing over time. The basin profiles seem to develop toward certain equilibrium asymptotically with time. Both the initial profiles show strong flood dominance, which is decreasing (at least, coming nearer toward the equilibrium line of equation (21)) when time proceeds. The position of the mouth is reasonably constant for t = 200 years and t = 800 years and the final profiles along the basin show the same parabolic shape as equation (21), which is represented by the solid line. However, the position of the mouth of the short basin deviates from the rest of the basin, which is attributed to the boundary condition not allowing for overtides. The long basin does not show this deviation near the mouth. This suggests that overtides do not play a significant role probably because of the larger depths at the mouth. Further the long basin is more flood dominant near the mouth and more ebb dominant landward.

[74] Measured values for sections of the Western Scheldt estuary derived by *Wang et al.* [1999] correspond only roughly to the values of the long shallow basin, see the dotted area in Figure 14b. Comparing the data with the model of Friedrichs and Aubrey, Wang observed that the data for the Western Scheldt did indeed correspond with the flood dominant character of certain sections, but data with relatively small values of a/h (<0.17) and Vs/Vc (<0.04) were characterized by ebb dominance in reality, which does not correspond with the flood dominant character predicted by the model.

4. Discussion

[75] The following section addresses major issues arising from the previous sections and discusses these in more detail.

4.1. Two Timescales

[76] Two timescales can be distinguished in the 2-D results that are related to the spatial scale of the phenomena taking place. The channel-shoal pattern with a spatial scale

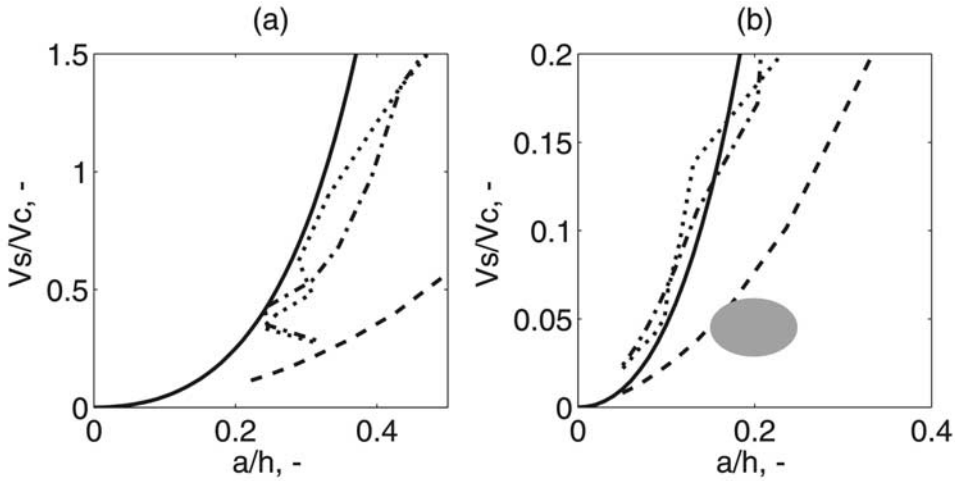

Figure 14. V_s/V_c versus A/h along the basin (left, down near the mouth; top right, more landward) for different points in time. Dashed line denotes initial profile, dash-dotted line denotes profile after 200 years, dotted line denotes profile after 800 years, and solid line represents equation (21). (a) 2.5 km wide short basin and (b) 2.5 km wide long, shallow basin. The shaded area represents data from sections in Western Scheldt from *Wang et al.* [1999].

of O(1–10 km) typically develops within the first 100 years (see Figure 13). After that, development still takes place, but with an increasingly slower rate related to the second timescale. Hypsometric plots that hardly develop over time shown in Figure 12 confirm this observation. The second timescale is related to the development of the width-averaged longitudinal profile with a spatial scale related to the basin width O(10–100 km). Depending on the initial bed, the longitudinal profile adaptation rate varies from centuries to millennia. For the long shallow basin, for example, the lowering of the average bed level in the basin takes place with a (slow) rate of approximately 4 m in 1600 years.

[77] The two distinct timescales were also reported by *Tambroni et al.* [2005] who experimented in a laboratory flume with a long channel, closed at one end and attached to a basin with a varying water level at the other end. They investigated two model configurations, namely a rectangular basin and a basin with an exponentially decaying width. Bed patterns developed already in the first 50 tidal cycles and take the form of an alternating bar pattern, just like in the current model results. Equilibrium of the width-averaged longitudinal bed profile was reported only after 2000 tidal cycles. Just as the current model results, the resulting end profile was concave at the seaward end and slightly convex at the landward end with a shoal forming at the head.

[78] It is suggested that pattern development is dominantly determined by local hydrodynamic conditions, which are relatively constant in time and may vary on a timescale that is much larger than the typical timescale of patterns formation. On the other hand, the development of the longitudinal profile is determined by a feedback process between the profile itself and the tidal behavior within the embayment, which characteristic length scales are of the same order of magnitude (80 km for the basin and a tidal wavelength of $L = Tc = T\sqrt{(gh)} \approx 12 * 3600\sqrt{(10 * 8 = 400}$ km)). This may explain the long timescale and the fact that no equilibrium was reached after 1600 years.

4.2. Pattern Formation

[79] By its two-dimensional nature the model introduces both longitudinal and lateral velocities and sediment transports, thus allowing growth of bars and tidal flats. The morphological patterns resemble observations in nature [*Van Veen*, 1950; *Ahnert*, 1960; *Dalrymple and Rhodes*, 1995] and earlier results of 2-D modeling by *Schramkowski et al.* [2004] and *Hibma et al.* [2003c].

[80] Equation (15) relates hydrodynamic and morphodynamic model parameters to a characteristic morphological wavelength. The relation of a typical morphological length to the tidal excursion is also found by *Hibma et al.* [2003b, 2003c] and *Schramkowski et al.* [2002]. More specifically, the tidal excursion divided by a characteristic timescale (tidal period (T)) scales with a characteristic tidal velocity. The higher this velocity is, the longer distance a sand particle will travel during flood or ebb.

[81] The linear impact of the water depth can be hydrodynamically related to the magnitude of the inertia of the water mass (see also equations (2) and (3)) just as in case of the characteristic tidal velocity described previously. Besides, there is a relatively small influence on friction via the value for c_f (see also equation (4)) stating that the magnitude of friction is less in deeper parts. Both effects support a larger morphological wavelength for larger ratios of inertia over friction.

[82] A relationship between basin width and a typical morphological wavelength (the meandering wavelength in this case) was also revealed (at least for initial bar formation) both by *Van Leeuwen and De Swart* [2004] using a numerical model and by *Yalin and Da Silva* [1992] on the basis of an inventory of empirical data of alternating bar length scales. The dependency on the basin width shows that the banks of the basin restrict the sinusoidal channel to develop longer and wider. However, the role of the basin width in the relatively short and wide basins, including multiple channels, is not clear. Although also

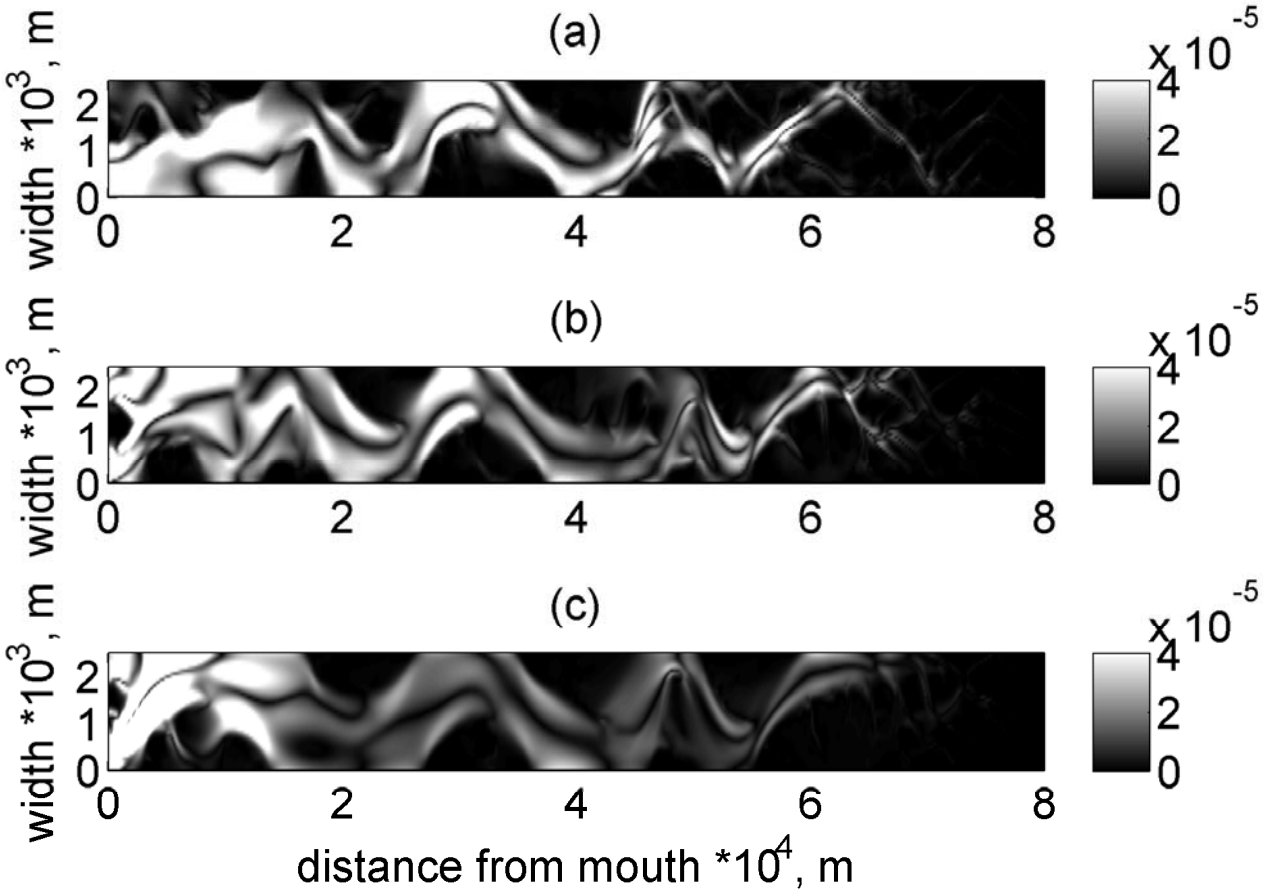

Figure 15. Magnitude (in m^3/sm) of tide-residual transport for long shallow basin after (a) 200, (b) 400 and (c) 800 years.

multiple channel systems could be under influence of the basin width, it is expected that there is somehow a maximum basin width that will influence the morphological wavelength.

[83] The dimensionless parameter (α_{bn}), see equation (9), influences sediment transport on a bed slope perpendicular to the flow direction. A higher value will flatten the cross-sectional profile of the basin, which allows for larger width scales of the bars and an increase of their length scales. Sensitivity analysis shows that increasing values for (α_{bn}) will increase the morphological wavelength at least by its root value.

[84] The dimensionless parameter (c_f) has a slightly more complex relation to the morphological wavelength because of the water depth present in the denominator, see equation (4). Sensitivity analysis revealed an inversely linear relation between commonly used values of Manning's coefficient (n) ranging from 0.02 to 0.03 $sm^{-1/3}$ and the morphological wavelength.

[85] *Struiksma et al.* [1985] carried out a linear perturbation analysis for a similar model formulation under fluvial conditions. They derived a relation between the product of the longitudinal wave number ($k_r = \frac{2\pi}{L_{mw}}$) and an adaptation length of the flow ($\lambda_w = \frac{1}{2c_f}\overline{h}$) and the ratio of the adaptation length of the bed topography ($\lambda_s = \frac{1}{\pi^2}\frac{B^2}{\overline{h}} f_s\theta$) and the adaptation length of the flow (λ_w), where ($f_s\theta$) represents a bed slope effect comparable to factors (α_{bn}) and (α_s) of the current model. For the range of the current model values the relationship can be represented in approximation by

$$\lambda_w \lambda_s = \frac{1}{k_r^2} \tag{22}$$

[86] This leads to the following expression for the morphological wavelength:

$$L_{mw} = \frac{B}{\pi}\frac{\sqrt{f_s\theta}}{c_f} \tag{23}$$

[87] The expression was derived for fluvial conditions with a constant mean water depth and constant velocity. Both parameters form the zero-order solution, explaining their disappearance in equation (23). Also, a fixed transverse wave number of ($\frac{\pi}{B}$) was imposed across fixed banks leading to a prescribed alternating bar pattern. This alternating bar pattern excludes the possibility of multiple channels in a cross section apparent in the current model and would explain the proportionality with (B) instead of ($\sqrt{B}$) like in equation (15).

[88] Further, *Ikeda et al.* [1981] derived the following relation for river meandering length estimation based on a

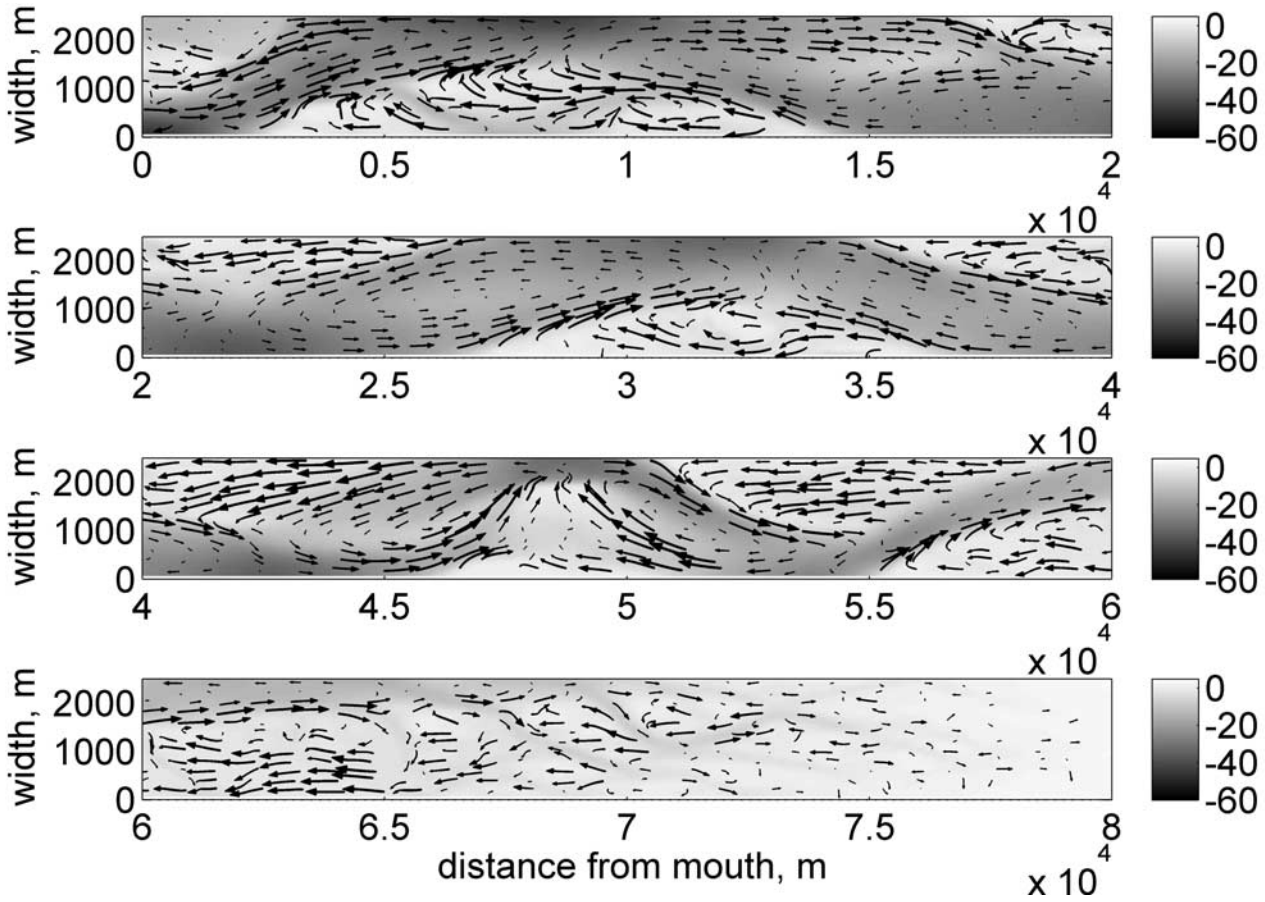

Figure 16. Map of (in surface) bed levels and (in vectors) the ratio of the tide residual sediment transport over the local RMS value of the sediment transport for the long shallow basin combined with a bed level after 800 years. The former indicates the dominant direction of the local sediment transport.

stability analysis of a fluvial sinuous channel with erodible banks:

$$L_{meanderlength} = \frac{\pi}{0.75}\frac{\overline{h}}{c_f} \tag{24}$$

[89] Although the relationship between alternating bar length and meandering length may not be straightforward [see also *Ikeda et al.*, 1981], equation (24) shows a certain resemblance with equation (15).

[90] In both latter equations based on stability analysis, the velocity vanishes contrary to equation (15). The reasons for this might be that the velocity is not constant in longitudinal direction along the basins, because of nonlinear interaction with the concave shape of the bed, friction and the tidal behavior in basins that are not short.

[91] The current analysis shows that model parameters can be qualitatively and quantitatively related to a characteristic morphological wavelength. However, at this moment no explanation was found for the dimension of coefficient (δ). Additional research could clarify this as well as the influence of the size of the grain diameter, a grain size distribution and a different sediment transport formulation. Additionally, validation of the relationship with physical observations would need to take place.

4.3. Comparison of 1-D and 2-D Longitudinal Profiles

[92] *Boon and Byrne* [1981], *Van Dongeren and De Vriend* [1994], *Friedrichs and Aubrey* [1996], *Schuttelaars and De Swart* [1996, 2000], *Lanzoni and Seminara* [2002] and *Hibma et al.* [2003a] showed that morphodynamic equilibrium can be reached using 1-D models that include width-averaged longitudinal depth profiles.

[93] Especially near the head, all 2-D basins corresponded quite well with 1-D model results. Only the shallow, long basin generated substantially more sedimentation near the head. This is attributed to the fact that (too) much sediment was available in the basin.

[94] Just as the 1-D model results, all 2-D basins show a slightly concave longitudinal profile, despite the disturbance by the pattern formation (see Figure 8). This is remarkable, since research by *Friedrichs and Aubrey* [1988] suggests that the intertidal area will significantly influence the behavior of the tidal wave and the related sediment transports within the basin. However, the criterion for morphodynamic equilibrium by equal ebb and flood duration [*Dronkers*, 1998] may be finally fulfilled for the 1-D (excluding intertidal area) and 2-D (including intertidal area) configurations, despite their different dominant mechanisms. As an illustration, Figure 14a indicates that the short basin has reached a certain equilibrium in terms of the

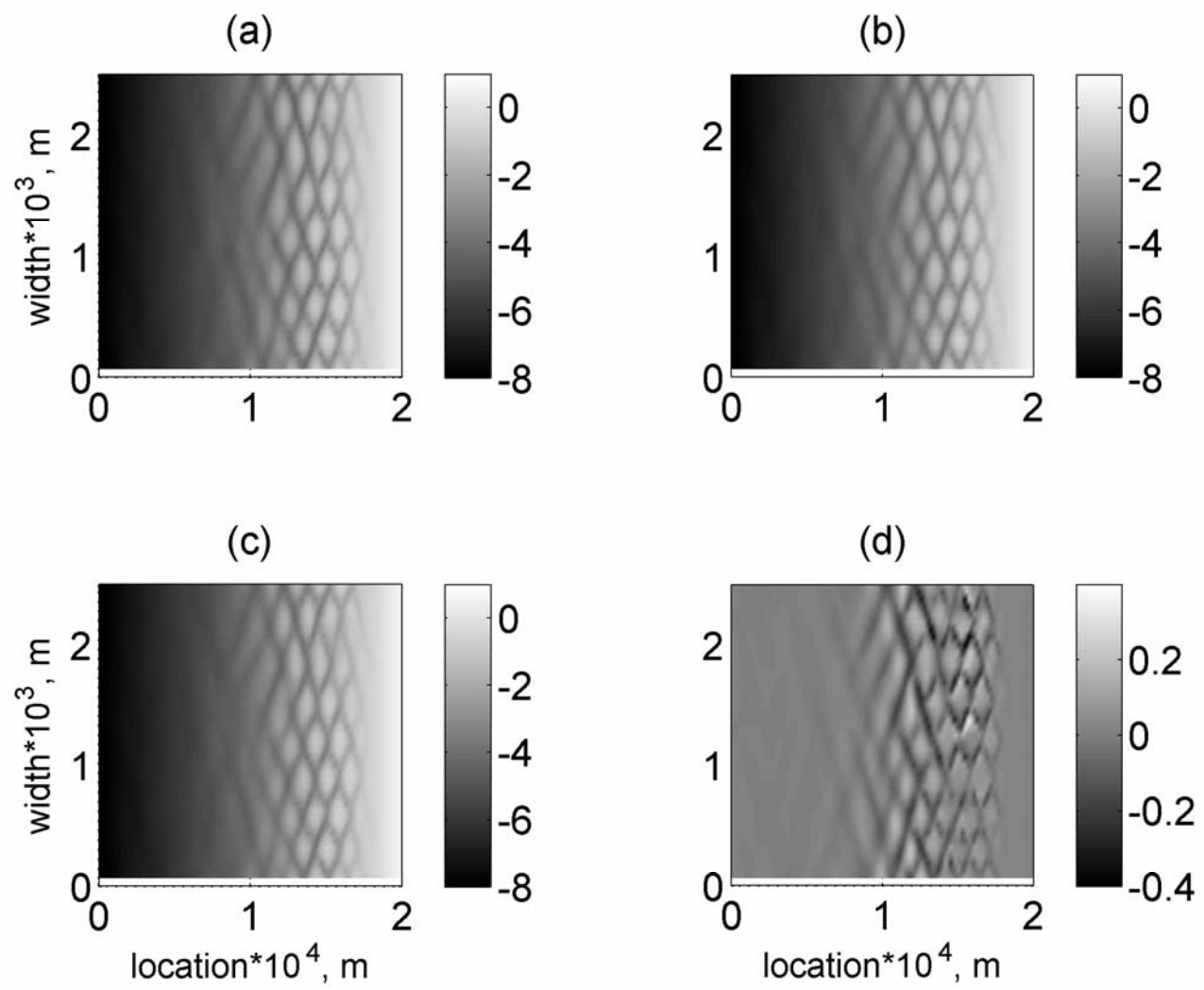

Figure 17. Bed levels of short 2.5 km wide basin after 20 years: (a) results with MF of 1, (b) difference between MF 1 and MF 10, (c) results with MF 400, and (d) difference between MF 1 and MF 400.

relatively constant value for the (a/h) versus (Vs/Vc) relationship after 200 years at the mouth.

[95] However, the 2-D bed levels at the mouth tend to be higher for all basins except for the long deep basin. This effect does not seem to disappear over time (see Figure 8). Furthermore, it is observed that one relatively deep channel is persistently present at one side of the basin at the mouth and that the rest of the mouths' cross section is generally covered by a shoal. Since these phenomena seem to be an effect only taking place near the mouth in both the short and long basins, it may be possibly attributed to the numerical formulation of the boundary condition, especially where it concerns the presence of intertidal area. Apparently, for the highly schematized boundary condition (both in terms of hydrodynamics and morphodynamics), the patterns cause flow conditions that favor relatively shallow width averaged bed levels, compared to 1-D situations without pattern development.

4.4. Tide Residual Sediment Transport

[96] A possible indication for reaching morphodynamic equilibrium is a disappearing tide residual sediment transport over time. Figure 15 shows the magnitude of the tide residual transport for the long, shallow basin for different points in time. Main transports take place in the channels. The residual transports decrease along the basin over time although the major transports at the mouth still differ at least an order of magnitude with the rest of the basin. The direction of the residual transports becomes clear in Figure 16 showing the bathymetry and the residual transport made dimensionless per cell by the RMS value of the sediment transport over one tide per cell for the long shallow basin after 800 years. It is apparent that the ebb dominant transport is maintained on the shoals and at the landward side of the shoals and that flood dominance occurs at the seaward side of the shoals and in the channels. Although the gross transport may be high in the deeper parts of the channel (see Figure 15), the dimensionless residual transport in the channel is small apart from the area near the mouth. On the shoals the dimensionless residual transport is high compared to that in the deeper parts of the channels. A circulating pattern can be distinguished (particularly between km 42 and 49) that flows

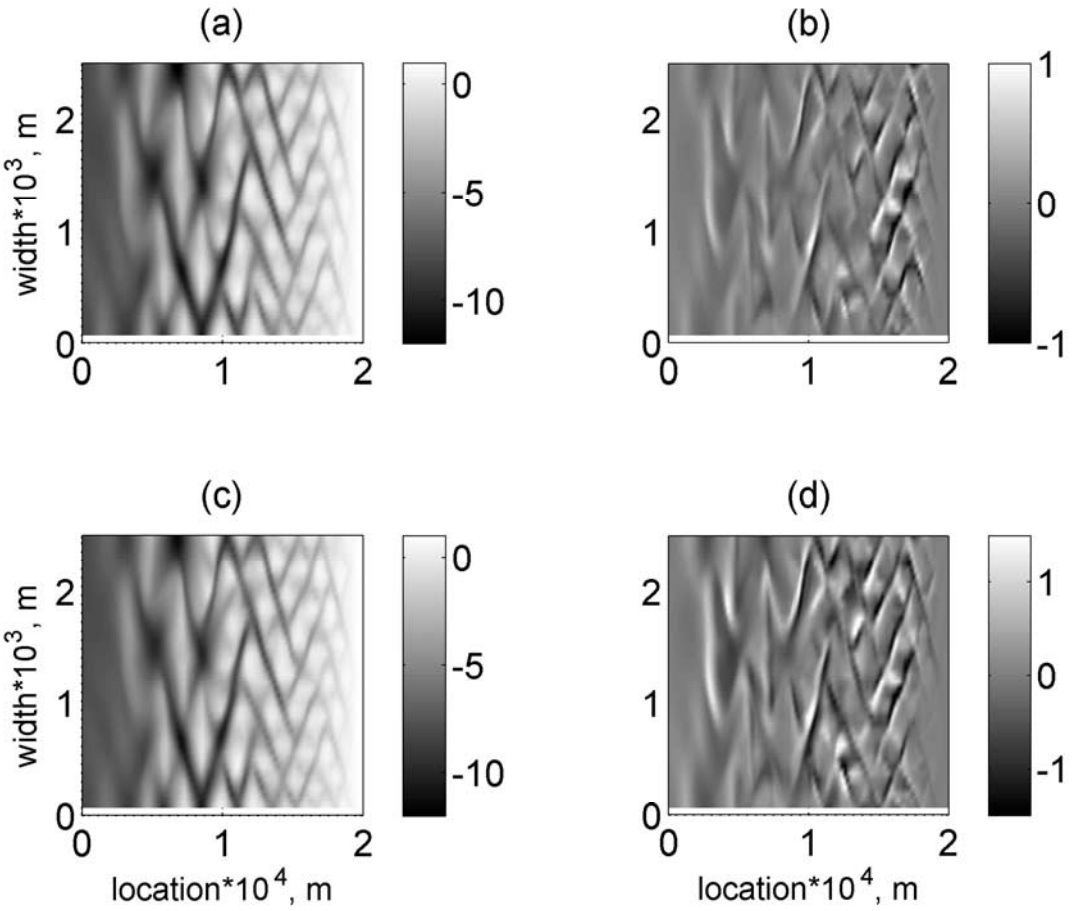

Figure 18. Bed levels of short 2.5 km wide basin after 100 years: (a) results with MF of 10, (b) difference between MF 10 and MF 400, (c) results with MF 1000, and (d) difference between MF 10 and MF 1000.

laterally from the shoals to the deeper parts of the channel and longitudinally from the deeper parts of the channel toward the shoals. The reason for this was investigated by *Coevelt et al.* [2003] who concluded that it originates from a water level set up in the channel bends.

4.5. Boundary Condition

[97] The boundary condition at the mouth is defined by a sine shaped water level with a period of 12 h, only slightly deviating by 42 min from the M_2 tidal period. This simple definition, however, raises a number of questions.

[98] The water level boundary was used since it makes comparison possible with earlier research by *Lanzoni and Seminara* [2002], *Hibma et al.* [2003a] and *Schuttelaars and De Swart* [1996, 2000]. The latter and *Van Dongeren and De Vriend* [1994] also investigated the impact of overtides (M_4 in relation to M_2) present in the definition of the boundary and concluded major impact on the sediment export/import of the basin depending on the value of the overtides amplitude and its phase difference with M_2. *Friedrichs and Aubrey* [1988] systematically investigated these impacts on the basis of measurements and a model of a highly schematized short basin. *Dronkers* [1998, 2005] even states that the existence of tidal basins in the Netherlands can be fully attributed to the character of the tide generated at the foreshore; certain ratios of the M_2/M_4 water level tide will always lead to flood dominant, estuaries, filling the basins with sediment and forcing river flows to find an outlet where conditions of the M_2/M_4 ratio are more favorable. For the current research, the authors choose not to investigate the impact of boundary condition overtides, since it would logically require numerous and lengthy 2-D runs.

[99] Figures 8a and 8b show decreasing width-averaged depths at the mouth for the 2-D model and increasing depths for the 1-D model. Although, all basins continue to export sediment toward the sea which is shown in Figure 9. This leads to the conclusion that the consequences of the water level definition of the boundary are not clear. Although the water level boundary is purely sine-shaped, the velocity asymmetry and its phase difference with the water level plays a dominant role in the basins' import or export. This will be investigated in more detail by M. Van der Wegen et al. (Long-term morphodynamic evolution and energy dissipation in a coastal plain tidal embayment, submitted to *Journal of Geophysical Research*, 2007, hereinafter referred to as Van der Wegen et al., submitted manuscript, 2007).

[100] Another point of discussion is that the definition of the boundary, in principle, consists of a signal of an incoming tidal wave and an outgoing tidal wave. The

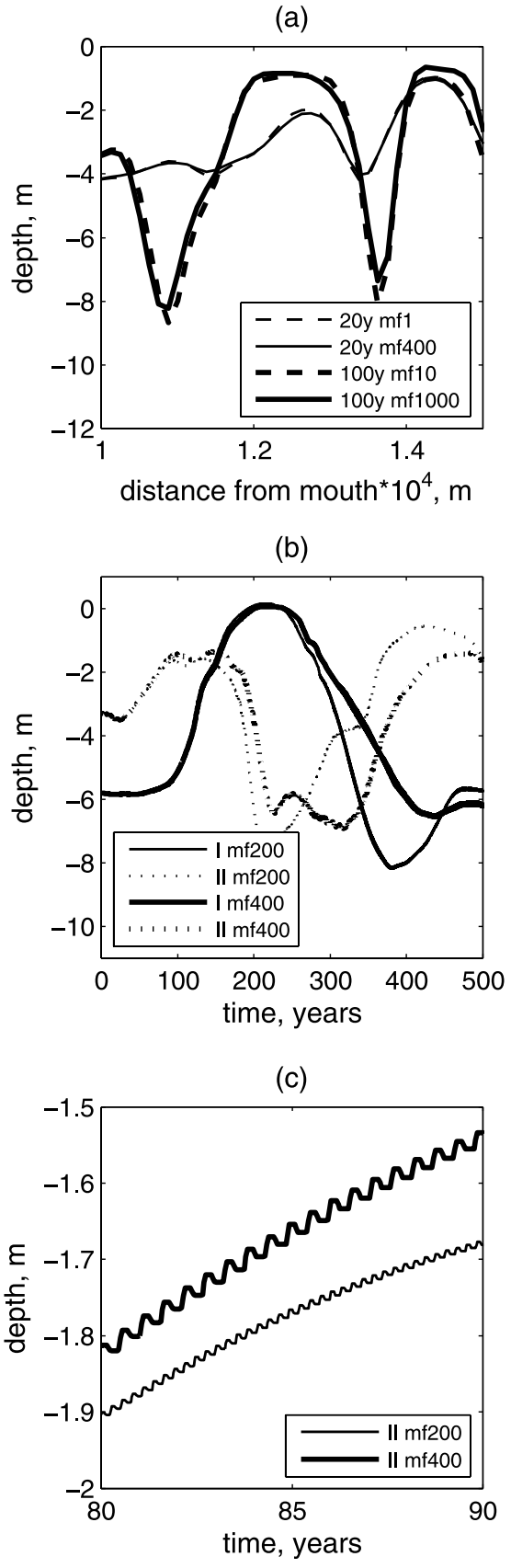

incoming part of the wave enters the basin, where it is subject to friction, and reflects against the head before going out of the basin again. In case of a deeper basin the impact of friction will become less and more wave energy is reflected against the head and moves out of the basin. In this way, the prescribed water level boundary implicitly means that, by a deepening and deforming basin during the model run, the incoming wave energy decreases. It is assumed in the current research that this effect is negligible, although further research should reveal the impact of this effect.

4.6. Morphological Update Scheme

[101] The validity of the results obtained in this study depend on a proper performance of the morphological update scheme applied. Figure 4c showed already that, for the 1-D schematization, values of the morphological factor up to 400 did not significantly lead to different results compared to a morphological factor of 1. At this point it is worthwhile to take a closer look at the 2-D model results and to evaluate the impact of the approach. Figures 17 and 18 show a comparison of 2-D model results after 20 years and 100 years for different values of the morphological factor (MF). After 20 years the difference between MF 1 and MF 10 are negligible (Figure 17b). After 100 years a MF of 1000 (Figure 18c) even shows similar results to a MF of 10 (Figure 18a). Figures 17 and 18 show that higher MFs result in larger deviations, although this is mainly due to a small phase shift of the pattern characteristics. Figure 19a shows additionally that a high MF results in somewhat shallower channels. Figure 19b shows that local bed levels may differ on the longer timescale for different MFs although this is mainly attributed to the pattern phase shift.

[102] The principle of the online MF approach is clearly illustrated by Figure 19c as a detail of Figure 19b. Apart from the initial values the bed levels show similar evolution over time, despite the fact that the higher MF results in larger deviations (proportional to the values of the MF) during the tidal cycle. As long as the bed level differences during a tidal cycle and after one time step remain low compared to the water depth, the bed level update does not significantly influence the hydrodynamics and the online approach will lead to acceptable results.

[103] A final analysis was made on the effect of different values for the MF based on a bed level including pattern development (i.e., a bed level after 1600 years). Figure 20b presents the difference between MF 1 and MF 400 after 10 years, which shows the relatively small differences and the fact that the major differences are located at relatively high bed slopes.

[104] The question arises what value of the MF is acceptable. It was found that only occasionally and for local points the differences in bed level during a tidal cycle amounted up

Figure 19. Bed level development over time for different morphological factors for the short 2.5 km wide basin: (a) spatial plot of cross section in landward direction and (b) comparison of results of MF 200 and MF 400. Points were taken at 6 km (point I) and 11 km (point II) from the mouth and 500 m from the upper bank. (c) Detail of Figure 19b at point II.

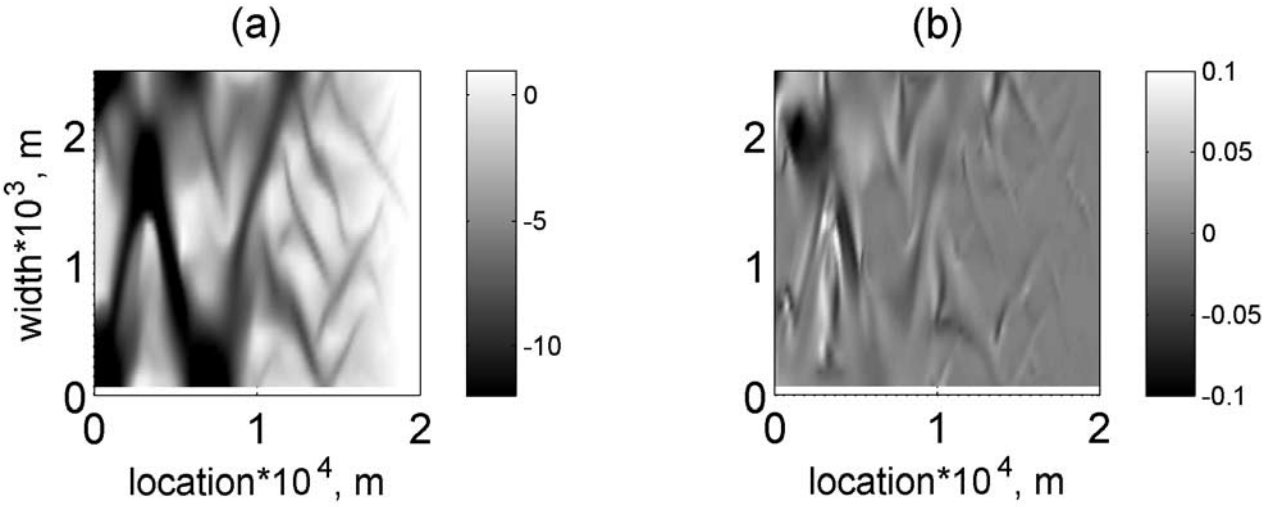

Figure 20. Bed levels of short 2.5 km wide basin based on 1600 year initial bed and results after 10 years: (a) results with MF 1 and (b) difference between MF 1 and MF 400.

to 25% of the water depth in case of a MF of 400. Larger values (i.e., 1000) were considered as unacceptable, because of the larger phase shift (see Figure 18d) and the larger amount of bed level points exceeding unacceptable bed level changes.

5. Conclusions and Further Research

[105] The current research addresses the evolution of an alluvial embayment using a numerical, process-based model. One-dimensional and two-dimensional schematizations were investigated for different configurations of the basin and their outcomes were compared to each other, to empirical relationships and data from the Western Scheldt estuary.

[106] The 1-D model results show that, although no equilibrium could be reached in a timeframe of 8000 years, the longitudinal profile shows strongly asymptotic behavior for two different initial bed levels. The shape of the profiles is similar and slightly concave and can be related to earlier research by *Schuttelaars and de Swart* [1996, 2000], *Van Dongeren and De Vriend* [1994] and *Lanzoni and Seminara* [2002] despite their different formulations for the sediment transport and the geometry of the basin.

[107] The 2-D results again show that equilibrium was not reached. However, distinction can be made between two timescales Pattern development is dominantly determined by local, relatively constant, hydrodynamic conditions with a timescale of decades, whereas the development of the longitudinal profile is determined by a feed back process between the profile itself and the tidal behavior within the embayment with a timescale of millennia. On the basis of the model results a relationship could be derived between a characteristic morphological wavelength and local tidal excursion, the local basin width and the width-averaged depth. Also a description of the hypsometry is suggested.

[108] The 2-D model results compare well with empirical relationships and data from the Western Scheldt in terms of the tidal prism versus the cross-sectional area and the channel volume versus the tidal prism at different locations along the basin. The scatter of the model generated data around the empirically derived relationships of *Jarret* [1976] and *Eysink* [1990] could mean that the dynamics of the system (both in the model and in reality) may fluctuate within an order of magnitude of the relationships, although additional research would be required to test this hypothesis.

[109] Also comparison of the model results to data from the Western Scheldt estuary leads to acceptable results in terms of morphological wavelength, the description of the hypsometry and the percentage of intertidal area. This is a remarkable result especially considering the fact that, among others, waves, grain size distribution, presence of mud and biomass, topographic features (such as dikes and peat layers present in the Western Scheldt) and the distinction between bed load and suspended load transport mechanisms were not taken into account.

[110] Comparing 1-D results with 2-D results shows similar longitudinal profiles. This is despite the fact that 2-D profiles are determined by different factors determining the tidal wave propagation characteristics, which include among others the shoal volume and channel depth.

[111] Major drawback of the current model is its definition of the boundary at the mouth, describing a sine shaped tide for the water level. Additionally, the rectangular shape of the basin does not correspond with exponentially decreasing estuary widths found in nature. Systematic observation of estuary geometry (e.g., by *Savenije* [2005]) shows generally an exponentially decaying width landward.

[112] Further research (M. Van der Wegen et al., submitted manuscript, 2007) will focus on a proper definition of the model boundary, the impact of erodible banks and decaying widths on long-term morphodynamic evolution as well as a more thorough analysis of the characteristic and changing hydrodynamic conditions within the basin.

[113] **Acknowledgments.** The authors would like to thank the editor and numerous anonymous reviewers for their valuable work and detailed discussion of the manuscript, in particular concerning the methodology of the morphodynamic update scheme. It certainly benefited the quality of our work.

References

Ahnert, F. (1960), Estuarine meanders in the Chesapeake Bay area, *Geogr. Rev.*, *50*, 390–401.

Bagnold, R. A. (1966), An approach to the sediment transport problem from general physics, *U.S. Geol. Surv. Prof. Pap.*, *422-I*.

Bates, P. D., and J. M. Hervouet (1999), A new method for moving boundary hydrodynamic problems in shallow water, *Proc. R. Soc. London, Ser. A*, *455*, 3107–3128.

Boon, J. D. (1975), Tidal discharge asymmetry in a salt marsh drainage system, *Limnol. Oceonagr.*, *20*, 71–80.

Boon, J. D., III, and R. J. Byrne (1981), On basin hypsometry and the morphodynamic response of coastal inlet systems, *Mar. Geol.*, *40*, 27–48.

Coevelt, E. M., A. Hibma, and M. J. F. Stive (2003), Feedback mechanisms in channel-shoal formation, in *Proceedings of the Fifth International Symposium on Coastal Engineering and Science of Coastal Sediment Processes, Coastal Sediments '03, ASCE, Clearwater Beach, Florida, USA* [CD-ROM], World Sci., Hackensack, N. J.

Dalrymple, R. W., and R. N. Rhodes (1995), Estuarine dunes and bars, in *Geomorphology and Sedimentology of Estuaries*, *Dev. in Sedimentol.*, vol. 53, edited by G. M. E. Perillo, pp. 359–422, Elsevier, New York.

Defina, A. (2000), Two-dimensional shallow water flow equations for partly dry areas, *Water Resour. Res.*, *36*, 3251–3264.

Dronkers, J. (1998), Morphodynamics of the Dutch Delta, in *Physics of Estuaries and Coastal Seas*, edited by J. Dronkers and M. B. A. M. Scheffers, pp. 297–304, A.A. Balkema, Rotterdam, Netherlands.

Dronkers, J. (2005), *Dynamics of Coastal Systems*, *Adv. Ser. on Ocean Eng.*, vol. 25, 520 pp., World Sci., Singapore.

Engelund, F., and E. Hansen (1967), *A Monograph on Sediment Transport in Alluvial Streams*, Teknisk Forlag, Copenhagen.

Eysink, W. D. (1990), Morphologic response of tidal basins to changes, paper presented at Coastal Engineering Conference, Am. Soc. of Civ. Eng., Delft, Netherlands.

Friedrichs, C. T., and D. G. Aubrey (1988), Non-linear tidal distortion in shallow well mixed estuaries: A synthesis, *Estuarine Coastal Shelf Sci.*, *27*, 521–545.

Friedrichs, C. T., and D. G. Aubrey (1996), Uniform bottom shear stress and equilibrium hypsometry of intertidal flats, in *Mixing in Estuaries and Coastal Seas*, *Coastal and Estuarine Stud.*, vol. 50, edited by C. Pattiaratchi, pp. 405–429, AGU, Washington, D. C.

Friedrichs, C. T., D. G. Aubrey, and P. E. Speer (1990), Impacts of relative sea-level rise on evolution of shallow estuaries, in *Residual Currents and Long-Term Transport*, *Coastal and Estuarine Stud.*, vol. 38, edited by R. T. Cheng, pp. 105–120, Springer, New York.

Hibma, A., H. M. Schuttelaars, and Z. B. Wang (2003a), Comparison of longitudinal equilibrium profiles in idealized and process-based models, *Ocean Dyn.*, *53*(3), 252–269.

Hibma, A., H. J. de Vriend, and M. J. F. Stive (2003b), Numerical modeling of shoal pattern formation in well-mixed elongated estuaries, *Estuarine Coastal Shelf Sci.*, *57*(5–6), 981–991.

Hibma, A., H. M. Schuttelaars, and H. J. de Vriend (2003c), Initial formation and long-term evolution of channel-shoal patterns, *Cont. Shelf Res.*, *24*(15), 1637–1650, doi:10.1016/j.csr.2004.05.003.

Ikeda, S. (1982), Lateral bed load transport on side slopes, *J. Hydraul. Div. ASCE*, *108*(11), 1369–1373.

Ikeda, S., G. Parker, and K. Sawai (1981), Bend theory of river meanders. Part 1. Linear development, *J. Fluid Mech.*, *112*, 363–377.

Jarret, J. T. (1976), Tidal prism-inlet relationships, *Gen. Invest. Tidal Inlets Rep. 3*, 32 pp., U.S. Army Coastal Eng. and Res. Cent., Fort Belvoir, Va.

Lanzoni, S., and G. Seminara (2002), Long-term evolution and morphodynamic equilibrium of tidal channels, *J. Geophys. Res.*, *107*(C1), 3001, doi:10.1029/2000JC000468.

Latteux, B. (1995), Techniques for long-term morphological simulation under tidal action, *Mar. Geol.*, *126*, 129–141.

Leendertse, J. J. (1987), A three-dimensional alternating direction implicit model with iterative fourth order dissipative non-linear advection terms, *WD-3333-NETH*, Rijkswaterstaat, The Hague, Netherlands.

Lesser, G. R., J. A. Roelvink, J. A. T. M. van Kester, and G. S. Stelling (2004), Development and validation of a three-dimensional morphological model, *Coastal Eng.*, *51*, 883–915.

O'Brien, M. P. (1969), Equilibrium flow areas of inlets on sandy coasts, *J. Waterw. Harbours Div.*, *ASCE 95*(WW1), 43–51.

Roelvink, J. A. (2006), Coastal morphodynamic evolution techniques, *J. Coastal Eng.*, *53*, 177–187.

Roelvink, J. A., T. van Kessel, S. Alfageme, and R. Canizares (2003), Modelling of barrier island response to storms, in *Proceedings of the Fifth International Symposium on Coastal Engineering and Science of Coastal Sediment Processes, Coastal Sediments '03, ASCE, Clearwater Beach, Florida, USA* [CD-ROM], World Sci., Hackensack, N. J.

Savenije, H. H. G. (2005), *Salinity and Tides in Alluvial Estuaries*, 194 pp., Elsevier, Amsterdam.

Schramkowski, G. P., H. M. Schuttelaars, and H. E. De Swart (2002), The effect of geometry and bottom friction on local bed forms in a tidal embayment, *Cont. Shelf Res.*, *22*, 1821–1833.

Schramkowski, G. P., H. M. Schuttelaars, and H. E. De Swart (2004), Nonlinear channel-shoal dynamics in long tidal embayments, *Ocean Dyn.*, *54*, 399–407.

Schuttelaars, H. M., and H. E. De Swart (1996), An idealized long term morphodynamic model of a tidal embayment, *Eur. J. Mech. B Fluids*, *15*(1), 55–80.

Schuttelaars, H. M., and H. E. De Swart (1999), Initial formation of channels and shoals in a short tidal embayment, *J. Fluid Mech.*, *386*, 15–42.

Schuttelaars, H. M., and H. E. De Swart (2000), Multiple morphodynamic equilibria in tidal embayments, *J. Geophys. Res.*, *105*(C10), 24,105–24,118.

Seminara, G., and M. Tubino (2001), Sand bars in tidal channels. Part 1. Free bars, *J. Fluid Mech.*, *440*, 49–74.

Speer, P. E., and D. G. Aubrey (1985), A study of non-linear propagation in shallow inlet/estuarine systems. Part II: Theory, *Estuarine Coastal Shelf Sci.*, *21*, 207–224.

Stelling, G. A. (1984), On the construction of computational methods for shallow water flow problems, *Rijkswaterstaat Commun.*, *35*, Rijkswaterstaat, The Hague, Netherlands.

Stelling, G. A., and J. J. Leendertse (1991), Approximation of convective processes by cyclic ACI methods, paper presented at 2nd Conference on Estuarine and Coastal Modelling, Am. Soc. of Civ. Eng., Tampa, Fla.

Struiksma, N. K., K. W. Olesen, C. Flokstra, and H. J. De Vriend (1985), Bed deformation in curved alluvial channels, *J. Hydraul. Res.*, *23*, 57–79.

Tambroni, N., M. Bolla Pittaluga, and G. Seminara (2005), Laboratory observations of the morphodynamic evolution of tidal channels and tidal inlets, *J. Geophys. Res.*, *110*, F04009, doi:10.1029/2004JF000243.

Van Dongeren, A. D., and H. J. De Vriend (1994), A model of morphological behaviour of tidal basins, *Coastal Eng.*, *22*, 287–310.

Van Leeuwen, S. M., and H. E. De Swart (2004), Effect of advective and diffusive sediment transport on the formation of local and global patterns in tidal embayments, *Ocean Dyn.*, *54*, 441–451.

Van Rijn, L. C. (1993), *Principles of Sediment Transport in Rivers, Estuaries and Coastal Seas*, 535 pp., AQUA Publ., Amsterdam, Netherlands.

Van Veen, J. (1936), *Onderzoekingen in de Hoofden* (in Dutch), Rijksuitgeverijdienst van de Ned. Staatscourant, The Hague, Netherlands.

Van Veen, J. (1950), Eb en vloed scharen in de Nederlandsche getij wateren, *J. R. Dutch Geogr. Soc.*, *67*, 303–325. (Engl. transl., Delft Univ. Press, Delft, Netherlands, 2002.)

Wang, Z. B., T. Louters, and H. J. De Vriend (1991), A morphodynamic model for a tidal inlet, in *Computer Modelling in Ocean Engineering '91*, edited by A. S. Arcilla et al., pp. 235–245, A. A. Balkema, Rotterdam, Netherlands.

Wang, Z. B., C. Jeuken, and H. J. De Vriend (1999), Tidal asymmetry and residual sediment transport in estuaries. A literature study and applications to the Western Scheldt, *Rep. Z2749*, WL|Delft Hydraul., Delft, Netherlands.

Yalin, M. S., and A. M. Da Silva (1992), Horizontal turbulence and alternate bars, *J. Hydrosci. Hydraul. Eng.*, *9*(2), 47–58.

J. A. Roelvink and M. van der Wegen, UNESCO-IHE Institute for Water Education, P.O. Box 3015, NL-2601 DA Delft, Netherlands. (d.roelvink@unesco-ihe.org; m.vanderwegen@unesco-ihe.org)